AD 767 879

A PRELIMINARY DESIGN OF A REMOTELY-
CONTROLLED GLIDER FOR A LONG-LINE
OPERATION

Elbridge Lee Snapp, III

Air Force Institute of Technology
Wright-Patterson Air Force Base, Ohio

June 1973

AD 767879

AIR FORCE INSTITUTE OF TECHNOLOGY

AIR UNIVERSITY
UNITED STATES AIR FORCE
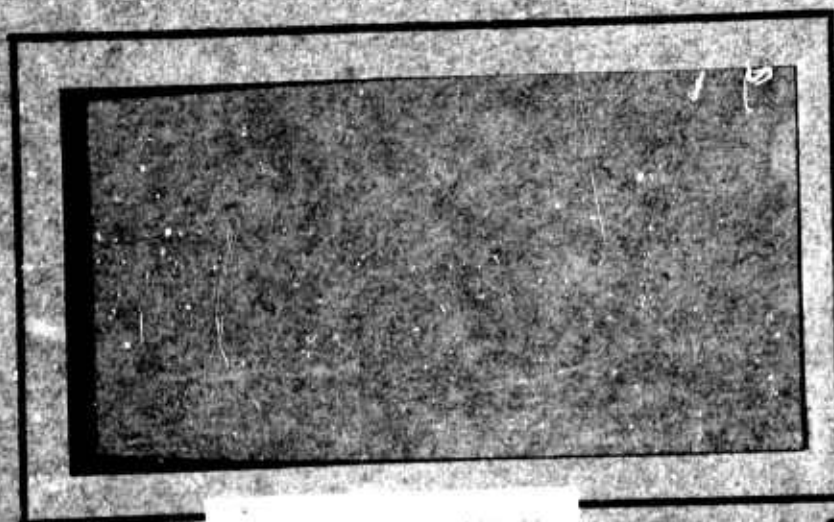
SCHOOL OF ENGINEERING

D D C

OCT 12 1973

C

WRIGHT-PATTERSON AIR FORCE BASE, OHIO

DOCUMENT CONTROL DATA - R & D

(Security classification of title, body of abstract and indexing annotation must be entered when the overall report is classified)

1. ORIGINATING ACTIVITY *(Corporate author)*	2a. REPORT SECURITY CLASSIFICATION
ir Force Institute of Tech logy (AFIT-EN) Wright-Patterson AFB, Ohio 45433	Unclassified
	2b. GROUP

3. REPORT TITLE

A Preliminary Design of a Remotely-Controlled Glider for a Long-Line Operation

4. DESCRIPTIVE NOTES *(Type of report and inclusive dates)*

AFIT Thesis

5. AUTHOR(S) *(First name, middle initial, last name)*

Elbridge L. Snapp, III
1Lt   USAF

6. REPORT DATE	7a. TOTAL NO. OF PAGES	7b. NO. OF REFS
June 1971	101	14

8a. CONTRACT OR GRANT NO.	9a. ORIGINATOR'S REPORT NUMBER(S)
b. PROJECT NO. N/A	GA/AE/71-1
c.	9b. OTHER REPORT NO(S) *(Any other numbers that may be assigned this report)*
d.	

10. DISTRIBUTION STATEMENT

Approved for public release; distribution unlimited.

11. SUPPLEMENTARY NOTES	12. SPONSORING MILITARY ACTIVITY
pproved for public release; IAW AFR 190-17 JERRY C. HIX, Captain, USAF Director of Information	

13. ABSTRACT

Low-level, covert observation of a small area of ground may be obtained by an unmanned glider towed from a large aircraft and suspended in Long-Line-Loiter. This glider is equipped with a Visually-Coupled Control System operated through a Low-Light-Level Television camera. The glider has a gross weight of 442.5 lb of which 282.3 lb is payload. The vehicle features a high wing and a constant-chord airfoil with 30 ft span. Overall vehicle length is 17.7 ft. Wings-level stall speed is 35.8 knots. The glider exhibits static longitudinal, lateral, and directional stability. Attaching the tow cable to the top of the fuselage above the vehicle center of gravity allows the glider to be flown in high-speed trail or suspended in Long-Line-Loiter.

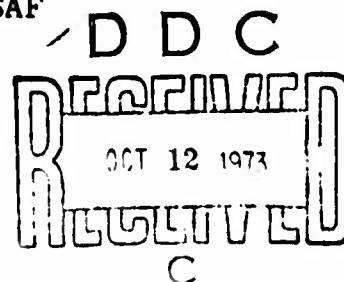| 14. KEY WORDS	LINK A		LINK B		LINK C	
	ROLE	WT	ROLE	WT	ROLE	WT
Remotely-controlled glider						
Long-Line-Loiter						
Glider preliminary design						

AD 767879

A PRELIMINARY DESIGN OF A

REMOTELY-CONTROLLED GLIDER FOR A LONG-

LINE OPERATION

THESIS

GA/AE/71-1   Elbridge L. Snapp, III
           1st Lieutenant   USAF

/D D C

RECEIVED

OCT 12 1973

C

ie

A PRELIMINARY DESIGN OF A
REMOTELY-CONTROLLED GLIDER FOR A LONG-
LINE OPERATION

THESIS

Presented to the Faculty of the School of Engineering

of the Air Force Institute of Technology

Air University

in Partial Fulfillment of the

Requirements for the Degree of

Master of Science

by

Elbridge L. Snapp, III, B.S.A.E.
1st Lieutenant   USAF

Graduate Astronautics

June 1979

iʃ

Preface

This thesis suggests a solution to the problem of obtaining low-level photoreconnaissance data with a recoverable instrument package. A preliminary design is proposed herein for a towed, unmanned glider carrying a Low-Light-Level Television.

Both the text and the appendices of this report contain an unusual amount of theoretical material. Well-established design procedures have been explained in detail. This was specifically directed to non-aerodynamicist users of the report.

Symbology throughout the thesis generally follows the notation of the USAF Stability and Control Datcom. The Datcom symbols were used whenever possible. Additional symbology was necessary, however, and it followed the Datcom style.

Many people gave freely of their time to assist the preparation of this thesis. I would like to thank my advisor, Professor Harold C. Larsen, Director, Air Force Institute of Technology Aerospace Design Center, who guided all phases of the work.

Lt. Col. John C. Simons and 1Lt. Eric Jumper of the Flight Environments Branch, Human Engineering Division, 6570th Aerospace Medical Research Laboratory, sponsored the project and supported it throughout. Mr. Charles Bates, Jr. and MSGT. Robert L. McMurry of the Performance Requirements

Contents

List of Figures

List of Tables

List of Symbols

Symbol	Meaning	Units
A	Aspect Ratio	
a	Three-Dimensional Wing Lift-Curve Slope	$(rad)^{-1}$
A_{eff_V}	Vertical Tail Effective Aspect Ratio	
a_o	Two-Dimensional Wing Lift-Curve Slope	$(rad)^{-1}$
$\bar{a}_o$	Average Two-Dimensional Lift-Curve Slope of a Twisted Wing	$(rad)^{-1}$
a_r	Rate of Change of Lift-Curve Slope of Horizontal Tail With Respect to Change in Rudder Deflection	$(rad)^{-1}$ $(deg)^{-1}$
ac	Aerodynamic Center	
A_W	Wing Aspect Ratio	
b	Wingspan	in, ft
c	Local (Section) Value of Wing Chord	in, ft
$\bar{c}$	Length of Wing Mean Aerodynamic Chord	in, ft
cc_l	Wing Section Lift Distribution	in, ft
cc_{l_a}	Wing Section Additional Lift Distribution for any C_L	in, ft
$cc_{l_{ax}}$	Wing Section Additional Lift Distribution for Wing of Variable Thickness for any C_L	in, ft
$cc_{l_{al}}$	Wing Section Additional Lift Distribution for $C_L = 1$	in, ft
C_D	Combined Vehicle Drag Coefficient	
C_{D_i}	Induced Drag Coefficient	
$C_{D_{pe}}$	Equivalent Pressure Drag Coefficient	
c_e	Elliptic Chord	

Symbol	Meaning	Units
c_f	Skin Friction Coefficient	
C_L	Wing Lift Coefficient	
c_l	Wing Section Lift Coefficient	
c_{l_b}	Wing Section Basic Lift Distribution	
$C_{L_{max}}$	Maximum Wing Lift Coefficient	
$c_{l_{max1}}$	Maximum Section Lift Coefficient for a Wing Lift Coefficient of 1.0	
c_{l_1}	Section Lift Coefficient for a Wing Lift Coefficient of 1.0	
C_{L_α}	Three-Dimensional Lift-Curve Slope	$(\text{rad})^{-1}$
$(C_{L_\alpha})_H$	Three-Dimensional Lift-Curve Slope of Horizontal Tail	$(\text{rad})^{-1}$
$(C_{L_\alpha})_V$	Three-Dimensional Lift-Curve Slope of Vertical Tail	$(\text{rad})^{-1}$
$(C_{L_\alpha})_{WB}$	Three-Dimensional Lift-Curve Slope of Wing-Body Combination	$(\text{rad})^{-1}$
C_{l_β}	Static Lateral Stability Derivative	$(\text{rad})^{-1}$
$(C_{l_\beta})_V$	Contribution of Vertical Tail to Static Lateral Stability Derivative	$(\text{rad})^{-1}$
$(C_{l_\beta})_W$	Contribution of Wing-Fuselage Interference Effect to Static Lateral Stability Derivative	$(\text{rad})^{-1}$
$C_{m_{ac}}$	Wing Moment Coefficient about Wing Aerodynamic Center	
C_{m_α}	Static Longitudinal Stability Derivative	$(\text{rad})^{-1}$
C_{n_β}	Static Directional Stability Derivative	$(\text{rad})^{-1}$
$(C_{n_\beta})_{fs}$	Contribution of Fuselage to Static Directional Stability Derivative	$(\text{rad})^{-1}$
$(C_{n_\beta})_V$	Contribution of Vertical Tail to Static Directional Stability Derivative	$(\text{rad})^{-1}$

Symbol	Meaning	Units
$(C_{n_\beta})_W$	Contribution of Sideslipping Wing Asymmetrical Lift and Drag to Static Directional Stability Derivative	$(rad)^{-1}$
C_{n_δ}	Rate of Change of Yawing Moment With Rudder Deflection	$(rad)^{-1}$ $(deg)^{-1}$
c_r	Length of Wing Root Chord	in, ft
c_t	Length of Wing Tip Chord	in, ft
$\bar{c}_V$	Length of Vertical Tail Mean Aero-dynamic Chord	in, ft
D	Drag	lbf
d	Maximum Fuselage Depth	in, ft
D_H	Drag Force of Horizontal Tail	lbf
E	Jones Edge Correction	
e	Aircraft Efficiency Parameter	
F	Force	lbf
g	Standard Sea Level Acceleration of Gravity	ft/sec^2
h	Mean Fuselage Depth	in, ft
$\hat{i}$	Unit Vector, Origin at Aircraft Center of Gravity, Positive Toward Nose	
$\hat{j}$	Unit Vector, Origin at Aircraft Center of Gravity, Positive out Right Wing	
K	Arithmetic Constant	
K	Correction Factor for Combined Parasite and Pressure Drags	
$\hat{k}$	Unit Vector, Origin at Aircraft Center of Gravity, Positive Down	
L	Lift	lbf
l	Length	in, ft
l_{ac}	Longitudinal Distance Between Aero-dynamic Center of Wing-Body and Aero-dynamic Center of Horizontal Tail	in, ft

Symbol	Meaning	Units
l_{fs}	Fuselage Length	in, ft
L_H	Lift Force of Horizontal Tail	lbf
l_H	Longitudinal Distance Between ¼ Mean Aerodynamic Center of Horizontal Tail and ¼ Mean Aerodynamic Chord of Wing	in, ft
l_{HC}	Longitudinal Distance Between Aircraft Center of Gravity and Aerodynamic Center of Horizontal Tail	in, ft
l_V	Longitudinal Distance Between ¼ Mean Aerodynamic Chord of Vertical Tail and ¼ Mean Aerodynamic Chord of Wing	in, ft
M	Mach Number	
M_{ac_H}	Horizontal Tail Pitching Moment About Horizontal Tail Aerodynamic Center	lbf-in lbf-ft
M_{ac_W}	Wing Pitching Moment About Wing Aerodynamic Center	lbf-in lbf-ft
M_{cg}	Moment About Aircraft Center of Gravity	lbf-in lbf-ft
n	Load Factor	g's
q	Dynamic Pressure	lbf/ft^2
q_V	Dynamic Pressure at Vertical Tail	lbf/ft^2
R	Radius of Turn	ft
R	Reynolds Number	
r	Fuselage Radius	in, ft
R_1	Reynolds Number Evaluated for a Wing Lift Coefficient of 1.0	
S_{B_S}	Fuselage Area in Longitudinal Section	in^2, ft^2
S_{fsG}	Gross Fuselage Surface Area	in^2, ft^2
S_H	Horizontal Tail Planform Area	in^2, ft^2
S_{HG}	Gross Horizontal Tail Surface Area	in^2, ft^2
SM	Static Margin	

Symbol	Meaning	Units
S_{TS}	Area in Longitudinal Section of Fuselage Aft Section	in^2, ft^2
S_V	Vertical Tail Planform Area	in^2, ft^2
S'_V	Area of Vertical Tail with the Area Extended to Fuselage Centerline	in^2, ft^2
S_{VG}	Gross Surface Area of Vertical Tail	in^2, ft^2
S_W	Wing Planform Area	in^2, ft^2
S_{wet}	Wetted Area	in^2, ft^2
$S_{wet_{ANT}}$	Antenna Wetted Area	in^2, ft^2
$S_{wet_{fs}}$	Fuselage Wetted Area	in^2, ft^2
S_{wet_H}	Horizontal Tail Wetted Area	in^2, ft^2
$S_{wet_{TH}}$	Tow Hitch Wetted Area	in^2, ft^2
S_{wet_V}	Vertical Tail Wetted Area	in^2, ft^2
S_{wet_W}	Wing Wetted Area	in^2, ft^2
$S_{wet_{WL}}$	Wheel Wetted Area	in^2, ft^2
S_{WG}	Wing Gross Surface Area	in^2, ft^2
T	Tow Line Tension	lbf
V	Velocity	ft/sec, knots
V_B	Fuselage Volume	in^3, ft^3
V_F	Effective Velocity Vector at the Fin	ft/sec
V_H	Horizontal Tail Volume Coefficient	
V_S	Aircraft Straight-Ahead Stall Speed	ft/sec, knots
V'_S	Aircraft Stall Speed in Coordinated, Constant-Altitude Turn	ft/sec, knots
V_V	Vertical Tail Volume Coefficient	
w	Mean Fuselage Width	in, ft
W	Weight	lbf

Symbol	Meaning	Units
x	Dimensionless Distance Increment for Region of Nonlinear Lift-Drag Relationship	
x	Distance Between Aircraft Center of Gravity and Wing Aerodynamic Center, Positive Rearward	in, ft
$\bar{x}$	Dimensionless distance of Wing-Body Aerodynamic Center Ahead of Aircraft Center of Gravity	
x_{ac}	Longitudinal Distance Between Wing Aerodynamic Center and Aircraft Center of Gravity	in, ft
x_c	Longitudinal Position of Aircraft Center of Gravity (Nose = 0)	in, ft
$\bar{x}_n$	Longitudinal Distance Between Aerodynamic Center of Wing-Body and Stick-Fixed Neutral Point	in, ft
x_R	Longitudinal Distance Between Tow Cable Attachment Point and Aircraft Center of Gravity	in, ft
y	Wing Span Station (Longitudinal Axis = 0)	ft % Span
z_R	Vertical Distance Between Tow Cable Attachment Point and Aircraft Center of Gravity	in, ft
z_V	Vertical Distance Between Mean Aerodynamic Chord of Vertical Tail and Aircraft Center of Gravity	in, ft
z_w	Distance Between Wing Root Chord and Fuselage Centerline Parallel to Aircraft z-Axis	in, ft

GREEK SYMBOLS

Symbol	Meaning	Units
α	Angle of Attack	rad, deg
α_{ZL}	Wing Zero-Lift Angle of Attack	rad, deg
β	Compressibility Parameter $\sqrt{1 - M^2}$	
β	Sideslip Angle	rad, deg

xiv

Symbol	Meaning	Units
Δ	Incremental Change	
δ_r	Rudder Deflection Angle	rad, deg
ϵ	Downwash Angle at Tail	rad, deg
ϵ_o	Wing Section Twist Angle	rad
η_H	Horizontal Tail Efficiency Factor	
κ	Ratio of Experimental Section Lift-Curve Slope to Theoretical Value, $2\pi/\beta$ at Same Mach Number	
$\Lambda_{c/4}$	Quarter Chord Sweep Angle	rad, deg
λ	Taper Ratio	
μ	Viscosity of Air	slug/ft-sec
ρ	Air Density	slug/ft^3
σ	Sidewash Angle	rad, deg
τ	Correction Factor for Induced Angle of Attack for Non-Elliptical Wing	
ϕ	Angle Measured at Tow Hitch Between Tangent to Tow Rope and Relative Wind	rad, deg

Abstract

Low-level, covert observation of a small area of ground may be obtained by an unmanned glider towed from a large aircraft and suspended in Long-Line-Loiter. This glider is equipped with a Visually-Coupled Control System operated through a Low-Light-Level Television camera. The glider has a gross weight of 442.5 lb of which 282.3 lb is payload. The vehicle features a high wing and a constant-chord airfoil with 30 ft span. Overall vehicle length is 17.7 ft. Wings-level stall speed is 35.8 knots. The glider exhibits static longitudinal, lateral, and directional stability. Attaching the tow cable to the top of the fuselage above the vehicle center of gravity allows the glider to be flown in high-speed trail or suspended in Long-Line-Loiter.

I. <u>Introduction</u>

To conduct combat operations successfully a commander must have at his disposal all available information concerning the enemy. Such information includes enemy troop strength, troop location, weapons, logistics, and avenues of advance and retreat. To be of use to the commander this information must be timely and obtained covertly. Traditionally, armies gathered combat intelligence by sending ahead small patrols. The advent of aircraft enabled airborne observers to obtain information more rapidly and accurately than before. The improvement of aerial photographic techniques made still more accurate reconnaissance data available.

Several problems remain to be solved, however, even with aircraft. An engine attracts the attention of those being observed. To protect himself from ground fire, the pilot must use either great speed or great height, neither of which may allow successful accomplishment of the desired mission. Observation of a very small location, for example a jungle clearing, might require a helicopter and camera crew. The disadvantages are obvious: a noisy engine invites gunfire. The closer the target must be observed, the greater the danger to aircraft and crewmembers.

The present study proposes one solution to this problem. This thesis is a preliminary aerodynamic study of a glider

which can be towed by a larger aircraft, for example a C-130. This glider carries a Low-Light-Level Television and associated equipment. At reduced light levels this equipment can gather low-level, low- and high-speed, covert photo-intelligence. The vehicle was designed to be remotely fly-able from the towplane by means of a Visually-Coupled Control System operated through the television camera. An operator located in the towplane can see through the tele-vision camera and can fly the glider using a remote control. Simultaneously, the data are collected for permanent record on a video tape.

The unmanned, towed glider combines several advantages which make this system very attractive:

1. The glider can be flown quite close to the ground without exposing personnel to small-arms fire. The length of the towline is to be about 5,000 feet. This puts the towplane high and out of the range of most small-arms fire.

2. The glider does not attract attention through engine noise.

3. The glider can be flown in high-speed trail to cover a wide strip, perhaps a road, at low level, or it may be flown in the Long-Line-Loiter mode so that it hovers nearly motionless over a point while the towplane orbits above.

4. If the appropriate personnel are carried aboard the towplane, data interpretation can be immediate.

5. The package is recoverable after the mission.

II. The Long-Line-Loiter

A technique called the Long-Line-Loiter is used to
suspend a body over a point on the ground. The body is
connected to a towing aircraft by a long cable and makes
no contact with the ground.

Figure 1, reproduced from Aeronautical Systems Divi-
sion Technical Report 69-95 (Ref 14:vii), shows the three
stages in the Long-Line-Loiter procedure. A payload, per-
haps simply a cone or other drag-producing device, is
attached to the free end of a cable which is typically
longer than 2,000 feet. The cable is drawn out to its full
length either with the aid of a small parachute, as shown
in Figure 1, or by simply releasing it out the back of the
towplane. At the appropriate time the pilot enters a pylon
turn which may be banked from 25 to 50 degrees. The lower
portion of the tow cable will stall and the payload, ideally,
will hang over a point on the ground. In practice, the
payload rarely hangs completely motionless, but describes
an irregular curve over a small area of ground while the
towplane orbits overhead. Irregularities in the payload's
path result from such perturbing forces as winds, air tur-
bulence, and inexact pilot technique. In addition to its
irregular ground track, the payload also bounces vertically
(Ref 14:1). Loiter times in a given small area are limited
by the endurance of the towing aircraft.

DELIVERY

LOITER

LAUNCH

(From Ref 14:vii)

Figure 1

Long-Line-Loiter Technique
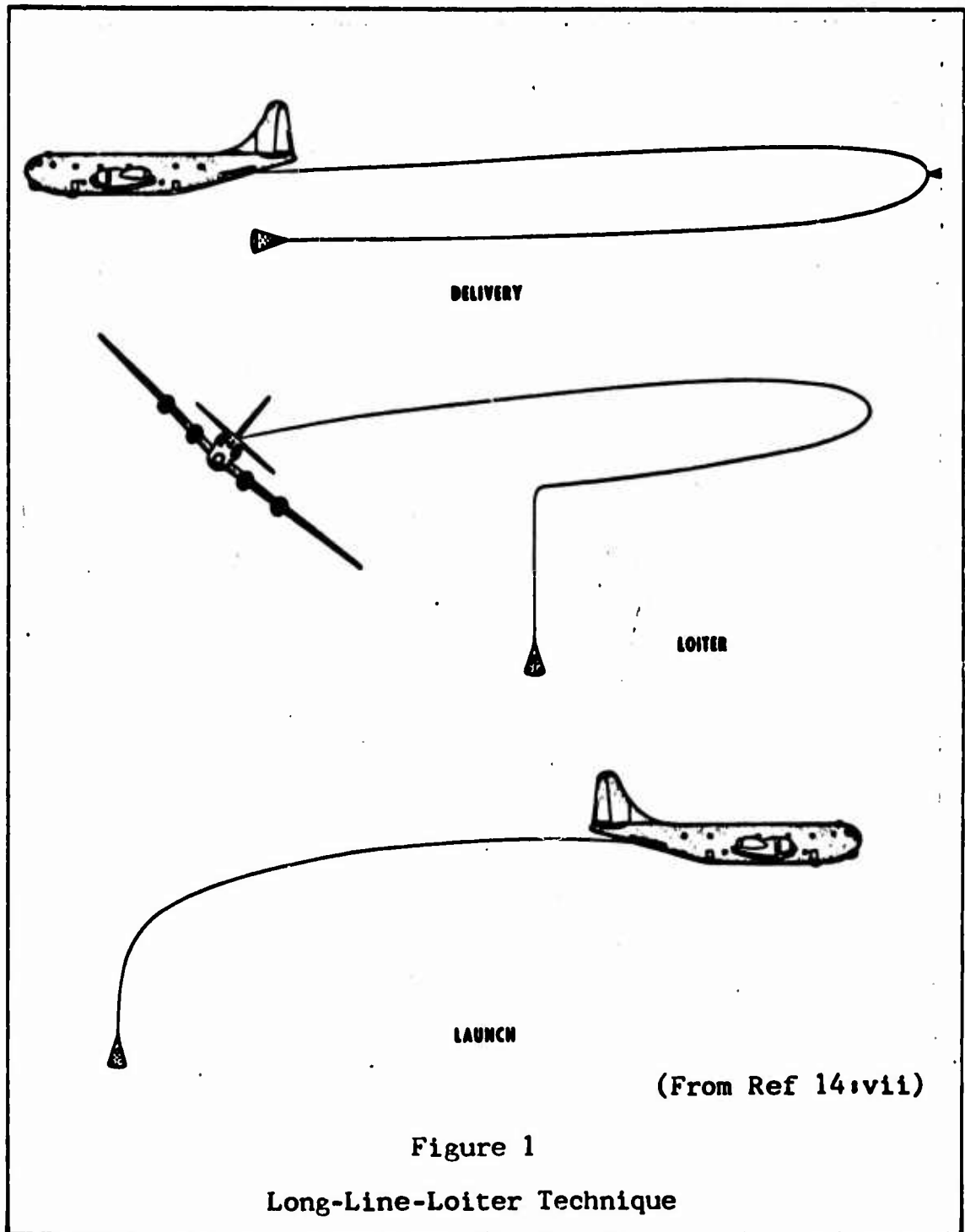
To recover the payload from Long-Line-Loiter, the pilot rolls the towplane to straight-and-level flight and pulls line and payload away. The line can then be reeled into the towplane to recover the payload. Applications of such a technique include precise pickup and delivery of instrument packages as well as personnel delivery and rescue (Ref 14:1).

III. Definition and Scope of the Problem

Design Specifications

The design specifications were presented by Lt. Col. John C. Simons of the 6570th Aerospace Medical Research Laboratory, Air Force Command, in May 1970. The problem was to design and study the aerodynamic characteristics of a towable drone meeting the following criteria:

1. Towable by a C-130 on a line 5,000 feet long.

2. Maneuverable 800 feet to either side of the tow aircraft while flying in trail 3,000 feet below the altitude of the tow aircraft.

3. Capable of controlled flight from 15 knots to 150 knots.

4. Capable of hanging nearly motionless while in Long-Line-Loiter, yet recovering to normal-attitude flight when the towplane leaves the Long-Line-Loiter mode.

5. Flyable at altitudes of from 25 feet above ground level (in Long-Line-Loiter) to 5,000 feet above ground level (full-speed trail).

Size, weight, configuration, aerodynamic parameters, and means of control were at the option of the designer.

Payload Selection

A tremendous variety of poential payloads exists for such a vehicle. Many types of cameras including conventional television, infrared, and Low-Light-Level Television

presently exist and are adaptable to the mission described above. Lt. Col. Simons suggested that the Low-Light-Level Television was the most useful system. Infrared was bulky, unreliable, and had excessive power requirements. Conventional television was less flexible than Low-Light-Level Television.

The Low-Light-Level Television was selected. Mr. Charles Bates, Jr., Supervisory Research Psychologist, Performance Requirements Branch, 6570th Aerospace Medical Research Laboratory, demonstrated the use and function of this system and showed its application to the project. MSgt Robert L. McMurry, Instrumentation Technician of the Performance Requirements Branch, prepared the block diagram of the Low-Light-Level Television system shown in Figure 2. Table I shows the size and weight of each component. Power requirements were to be met with a standard aircraft battery. This battery can generate in excess of 100 amps at 28 volts. An inverter converts the DC current to 400 cycles/sec AC current. The entire package requires between eight and nine amp-hours. At this rate battery life is about seven to eight hours. The television system is, therefore, self-contained in that no power need be delivered to it down the tow cable.

Vehicle Remote Control

If the vehicle were designed to have a fully-functioning set of conventional controls, it could be flown by remote control by an observer located in the towplane. However,
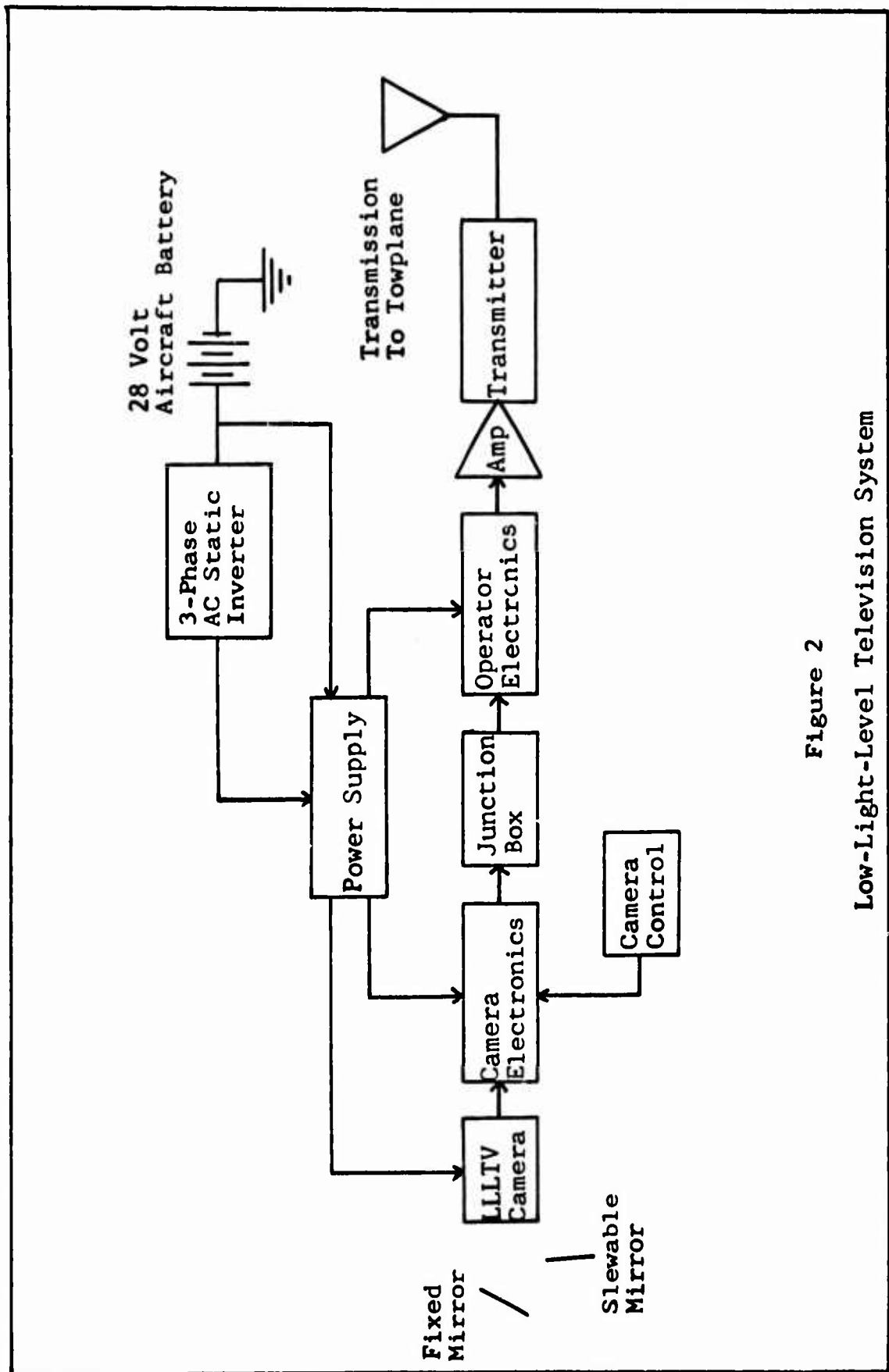
Figure 2

Low-Light-Level Television System

8

Table I

Sizes and Weights of the Components
of the Low-Light-Level Television System

Payload Item	Dimensions	Weight, lb
LLLTV Camera	12 in max dia	70.4
Camera Electronics	11 in X 14 in X 23 in	31.0
Aircraft Battery	12 in X 12 in X 12 in	80.0
Power Supply	14 in X 14 in X 23 in	70.4
Junction Box	6 in X 24 in X 28 in	29.9
Operator Electronics	14 in X 14 in X 23 in	23.0
Transmitter	6 in X 5 in X 2 in	2.2

suspended from a line 5,000 feet long, the vehicle would be nearly invisible to the operator expecially at low light levels, such as twilight. Control could only be accomplished if some means were found to "put the operator in the cockpit."

The Visually-Coupled Control System solves this problem. When an operator uses this system he wears a headset with small video receivers to allow him to see through the television camera. A sensor on the headset detects the operator's head position. When the operator moves his head, as though to look around him, the head position is relayed to a slewable mirror in the nose of the vehicle. The bottom of the nose is made of optical glass. The slewable mirror, moves to correspond to the operator's head position. The operator, looking through the camera, now has about the same vantage point that a hypothetical pilot might have, but with more restricted field of view. Finally, if the operator is equipped with a stick which transmits commands by radio signal to the controls, he can fly the vehicle.

The Visually-Coupled Control System combines two features:

1. It allows the operator in the towplane to fly the vehicle but to concentrate his vision anywhere in range of the slewable mirror.

2. Picking off the signal and feeding it onto video tape allows a continuous, permanent record to be made.

Scope of the Design

This thesis will present a preliminary design for a remotely-controlled, steerable drone. The drone will be a conventional glider with fully-functioning ailerons, elevator, and rudder. The major conclusions to be drawn from such a study are the shape and size of the vehicle and whether or not, aerodynamically, it will be flyable. No structural analysis is considered.

IV. Preliminary Weight Estimate

The initial step in the design process was to make a preliminary estimate of the gross weight of the vehicle. This estimate was obtained by

1. Breaking the aircraft up into its components.

2. Idealizing the components (fuselage becomes a cylinder, etc.).

3. Assuming sizes and skin thicknesses.

4. Computing the volume of material used.

5. Summing the weights represented by each component volume.

Professor Larsen suggested that considerable weight savings would result if the wing and fuselage were constructed as a foam sandwich. Instead of using the conventional ribbing inside the wing, the interior could be built using main and rear spars with the remaining space partly or completely filled with polyurethane foam which weighs 4 to 6 lb per cubic foot. This construction yeilds an extremely strong, lightweight wing to which a thin aluminum skin may be bonded.

Similarly, the fuselage could be constructed as a foam sandwich using two thin layers of metal separated by an inch-thick layer of foam. Such fuselage construction is capable of accepting large bending stresses while keeping the structural weight relatively small.

The preliminary weight estimate served only as an entry

point into the design iteration process and was not intended to be very accurate. However, an initial gross weight of 400 pounds was accepted as a starting point.

V. Configuration Buildup

Fuselage

The fuselage combines good aerodynamic characteristics with a simple layout for ease of manufacture. Figure 3 shows the arrangement of the items of payload within the vehicle. Payload items were located to place the center of gravity of the vehicle between 40% and 45% of the longitudinal axis (nose at zero datum) without regard for the ease of wiring the payload once installed.

The components are of diverse sizes. The minimum fuselage diameter must include the diagonal of the largest component plus additional allowence for the inclusion of interior structure. Table II lists the components and diagonal length of each piece of equipment. The junction box, due to its peculiar size (28 in X 24 in X 6 in), is the only component which cannot be included. Redesign of the junction box to a size of 12 in X 24 in X 14 in is suggested.

The fuselage is made up of three parts: a nose section 40 in long, a cylindrical main body 106 in long, and a tail section 40 in long. The fuselage is a body of revolution. The outside diameter of the cylindrical section was selected to be 28 in to allow ample clearance for interior structure. Overall fuselage length was set at 186 in. This is larger than required to contain the payload, but allows a smaller horizontal and vertical tail to

A. Fixed Mirror
B. Slewable Mirror
C. LLLTV Camera
D. Camera Electronics
E. Aircraft Battery
F. Power Supply
G. Junction Box
H. Operator Electronics
I. Transmitter
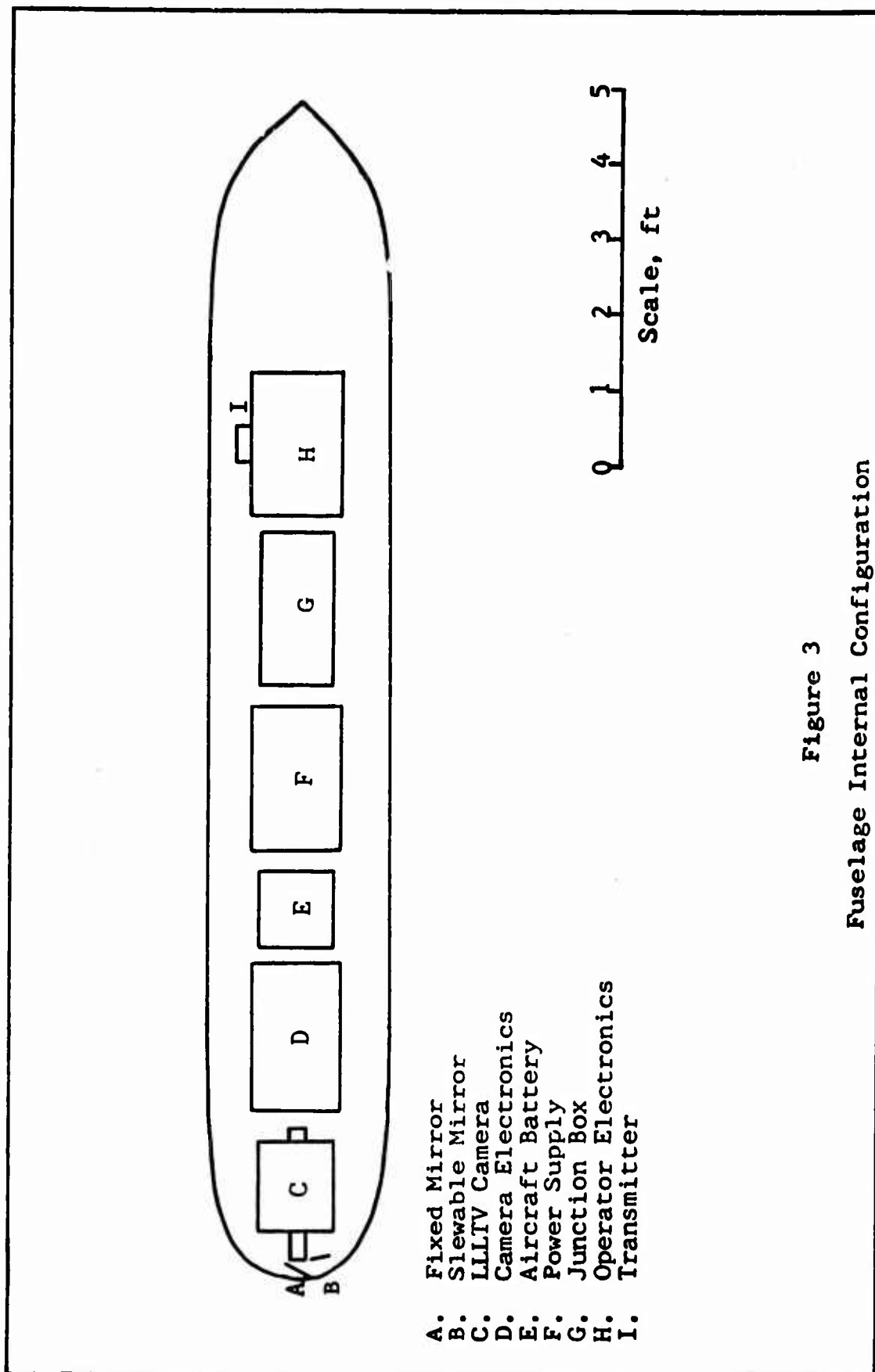
Figure 3

Fuselage Internal Configuration

> ### Table II
> #### Payload Diagonal Lengths
>
> | | |
> |---|---|
> | Power Supply | 19.8 in |
> | LLLTV Camera | 12.0 in |
> | Camera Electronics Box | 17.8 in |
> | Operator Electronics Box | 19.8 in |
> | Aircraft Battery | 17.0 in |
> | Junction Box (Original Size) | 24.7 in |

be used. With foam sandwich construction, the weight of the fuselage is estimated at 70 pounds.

The nose and tail sections were developed using the following equations:

Nose:
$$\left(\frac{x}{a}\right)^n + \left(\frac{y}{b}\right)^n = 1 \tag{1}$$

where, for this vehicle,

$$n = 3$$

$$a = 40 \text{ (length of nose section)}$$

$$b = 14 \text{ (maximum radius of fuselage)}$$

Tail:
$$\frac{d^2y}{dx^2} = Kx(1 - x) \tag{2}$$

Boundary conditions are:

$$\text{at } x = 0, \quad dy/dx = 0$$

$$\text{at } x = 40, \quad y = 14$$

Appendix A discusses the reasons for selection of these equations and their use in computing surface areas and volume.

Substituting the constants into Equation (1) and solving the boundary value problem (2) yield the equations for nose and tail.

Nose:
$$y = (2744 - 0.042875 x^3)^{1/3} \qquad (3)$$

Tail:
$$y = \frac{14}{2,432,000} (x^4 - 2 x^3) \qquad (4)$$

The area in longitudinal section (see Appendix A) is
$$S_{B_S} = 4856.6 \text{ in}^2 = 33.7 \text{ ft}^2$$

Multiplying the longitudinal section area by π gives the total external surface area for a body of revolution (Ref 1: 6:5). The external surface area is called the gross surface area, and it does not take into account that some of the surface is removed by intersection with wing and tail. The gross surface area of the fuselage is
$$S_{fsG} = 15,249.7 \text{ in}^2 = 105.9 \text{ ft}^2$$

The total fuselage volume is
$$V_B = 102,674.4 \text{ in}^3 = 59.3 \text{ ft}^3$$

Table III summarizes the fuselage parameters.

Wing

Airfoil Selection. The Clark Y airfoil section, plotted in Figure 4, was selected for this glider. The Clark Y is a low-speed, 12% thick airfoil with flat bottom surface and maximum thickness at one-third chord (Ref 9:9). The performance of the glider at airspeeds near the stall was considered to be the most important determining factor which influenced the decision. The Clark Y was selected

17

Table III

Summary of Fuselage Design Parameters

Shape	A Body of Revolution Consisting of Nose and Tail Sections and Cylindrical Center Body
Empty Weight	70 lb
Length	15.5 ft
Length of Nose Section	40 in
Length of Tail Section	40 in
Diameter of Cylindrical Section	28 in
Gross Surface Area	105.9 ft^2
Volume	59.3 ft^3
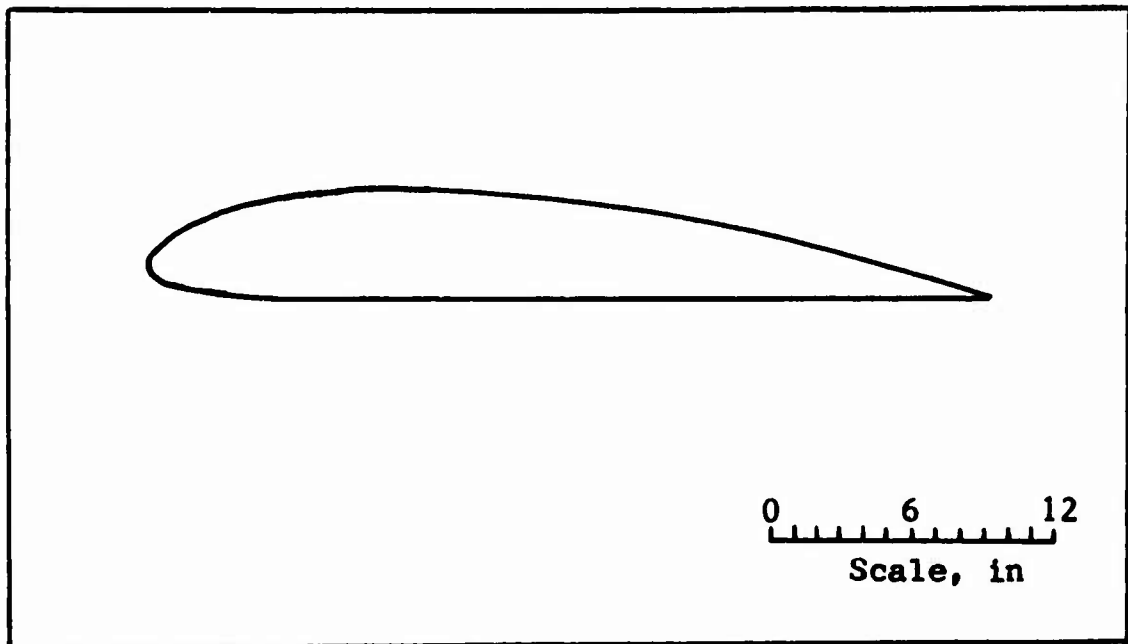
Figure 4. The Clark Y

for the following reasons:

1. It produces relatively high values of $C_{L_{max}}$.

2. It is a conventional airfoil long used in glider construction and has well-determined characteristics.

3. Its large thickness allows some latitude in the arrangement of internal structure.

4. It is relatively less sensitive to the effects of surface roughness than most other airfoil sections used in glider construction.

Dwinnell (Ref 5) has shown that the effects of surface roughness are seen in increased section drag coefficients. The low-drag airfoil, i.e., the glider airfoil, depends for its efficient operation upon maintaining laminar flow over a good portion of the surface of the wing. The laminar flow may be lost entirely if the airfoil surface is rough. For example the NACA 63_1-012, a low-drag section, may have

its section drag coefficient doubled at given section lift coefficient if the surface is roughened. A NACA 4415 airfoil flying near the stall may have its section maximum lift coefficient reduced by 0.30 to 1.25, precipitating stall at lower angles of attack solely due to surface roughness. Surface roughness may be due to the finish given the airfoil at the factory, but even a good finish may be seriously degraded by oil or dirt adhering to the wing (Ref 5:170, 171, 207). The Clark Y is not intended to be a low-drag airfoil, and the glider which uses it will not perform as a modern sailplane. However, the Clark Y is not nearly so susceptible to degraded performance due to surface roughness. During handling and maintenance, the wing surface will pick up nicks, scratches, and dirt. It will pick up splattered insects during the low-level portions of its flight. For these reasons the Clark Y is an appropriate airfoil for use in this design.

Airfoil Dimensions. The equation for stall speed as a function of wing loading is

$$V_S = \sqrt{\frac{2}{\rho\, C_{L_{max}}} \left(\frac{W}{S_W}\right)} \tag{5}$$

where the wing loading is (W/S_W). Low stall speeds are favored by low wing loadings. Increasing wing area decreases wing loading. Furthermore, as aspect ratio increases for a wing at given lift coefficient, wing drag coefficient decreases (Ref 2:3.15). Both of these factors indicate the

advantage of using large wing area and large aspect ratio.
The following wing dimensions were chosen for the vehicle:

Wingspan	30 ft
Wing Chord	3 ft
Aspect Ratio	10
Taper Ratio	1

The wing is an unswept, untwisted, constant chord Clark Y
without taper, dihedral, or flaps. The wing loading is
4.85 lb/ft^2.

Lift Distribution and Stall Point. Predicting the
stalling characteristics and maximum lift coefficient for
the wing requires the determination of the lift distribution
across the span. This was done using Schrenk's method as
presented by Pope (Ref 12). An explanation of Schrenk's me-
thod and its application to the present airfoil has been
included in Appendix B.

The section lift coefficient at any span station y
across the airfoil, is given by Equation (6).

$$c_1 = \frac{C_L}{c}\left[\frac{c}{2}\frac{a_0}{\bar{a}_0} + \frac{2S_W}{\pi b}\sqrt{1 - \left(\frac{2y}{b}\right)^2}\right] + \frac{\epsilon_0 - \alpha_{ZL}}{2}a_0 c \quad (6)$$

As shown in Appendix B, using the values selected for the
present airfoil, Equation (6) becomes

$$c_1 = \frac{C_L}{c}\left[1.5 + 1.908\sqrt{1 - \left(\frac{2y}{30}\right)^2}\right] \quad (7)$$

If the wing lift coefficient is set equal to 1.0, the section
lift coefficient becomes

$$c_{l_1} = \frac{1}{c} \left[1.5 + 1.908 \sqrt{1 - \frac{y^2}{225}} \right] \tag{8}$$

The lift distribution across the half-span was dtermined by assigning values to y from 0 to 15 ft. Figure 5 shows the lift distribution across the half-span for $C_L = 1$. The maximum possible wing lift coefficient may be found by scaling linearly from Figure 5. The stall point will occur at the maximum wing lift coefficient. A simple method for determining the stall point is as follows: The ratio of section $c_{l_{max}}$ to $c_{l_{max1}}$ may be expressed as

$$\frac{c_{l_{max}}}{c_{l_{max1}}} = \left(\frac{R}{R_1} \right)^p \tag{9}$$

where the exponent p is found to be

$$\frac{1}{12} \le p \le \frac{1}{8}$$

A value of 1/12 is appropriate for the Clark Y. The Reynolds Numbers were evaluated at chord length and stall speed and were approximately 1.5 millions. The Reynolds Number ratio is

$$\frac{R}{R_1} = \frac{c}{c_1} = 1 \tag{10}$$

The maximum lift coefficient for the Clark Y is 1.56 at R > 3 millions. At Reynolds Numbers of 1.5 millions, the maximum section lift cofficient expected for the Clark Y is 1.26. From
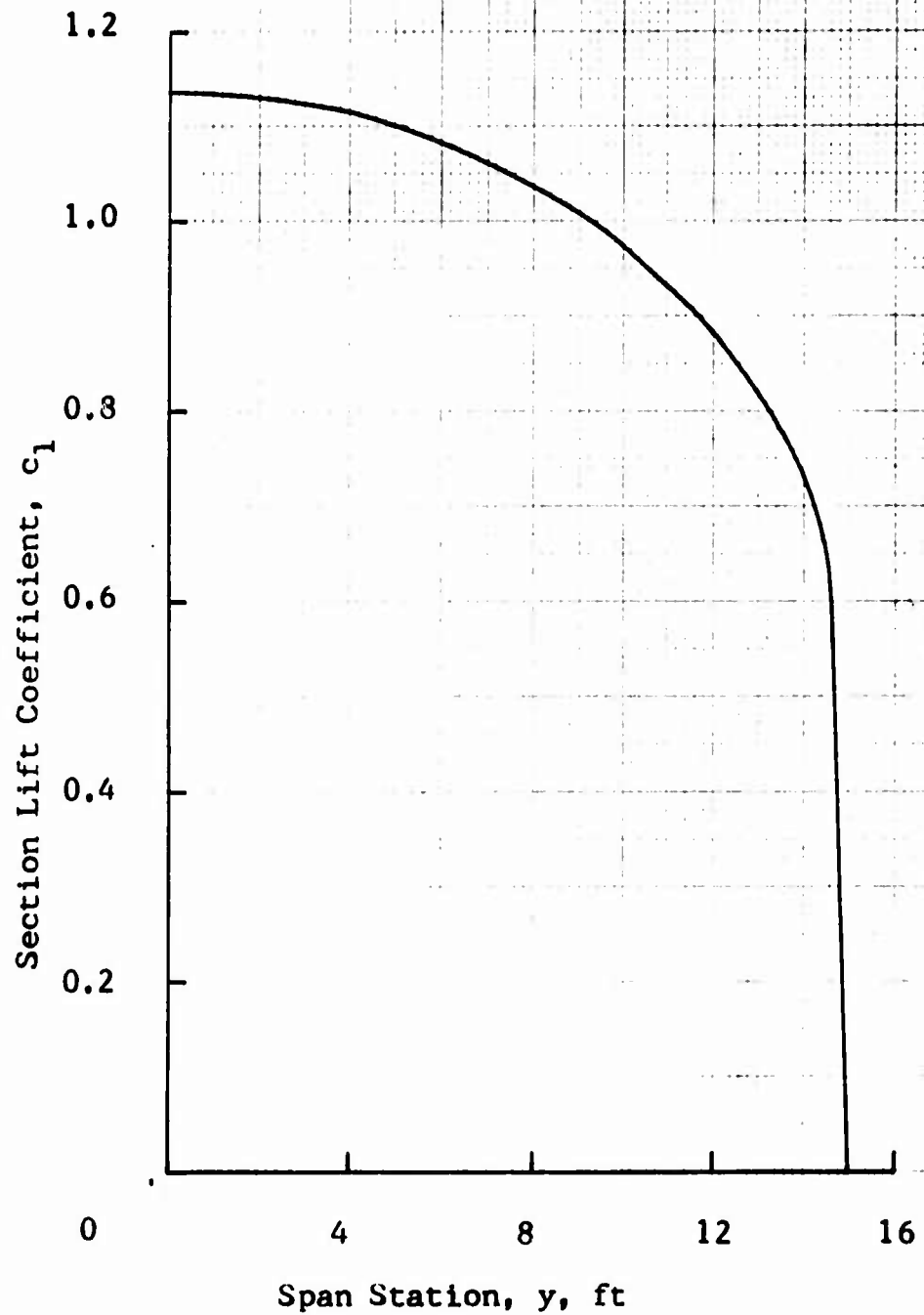
Figure 5

Lift Distribution Across the Half-Span

Figure 5, the maximum section lift coefficient is $c_{1_1} = 1.135$.
The maximum wing lift coefficient (C_L at stall angle of
attack) is

$$\frac{C_L}{C_{L_1}} = \frac{c_{1_{max}}}{c_{1_{max1}}} = \frac{1.26}{1.135} = 1.11$$

or, $C_L = 1.11$, since $C_{L_1} = 1.0$ by hypothesis. This value is
achieved first at the wing root The stall begins at the
root and moves outward along the span.

Slope of the Lift Curve. The slope of the lift curve
may be determined using other published data. The 1948
edition on NACA Report No. 669 (Ref 9:9) presents data
for a Clark Y of rectangular planform measuring 5 in X 30 in.
The lift-curve slope of this wing may be determined graph-
ically to be

$$a = 4.01 \ / \ \text{radian}$$

This three-dimensional value may be converted to the tow
dimensional value using Equation (11).

$$a_o = \frac{aE}{1 - \dfrac{a}{\pi A_W}(1 + \tau)} \qquad (11)$$

E is the magnitude of the Jones Edge Correction which
corrects the lift-curve slope of the finite wing for the
effects of spanwise flow. E is given by (Ref 12:207, 08)

$$E = \frac{\text{Wing Perimeter}}{2 \ (\text{Wing Span})} \qquad (12)$$

and $\tau = 0.17$ (Ref 2:3.17). The two-dimensional lift-curve
slope is

$$a_o = 5.50 \text{ / radian}$$

Equation (11) may be solved for the three-dimensioal lift-curve slope, a, to obtain

$$a = \frac{a_o}{E + \dfrac{a_o}{\pi A_W}(1 + \mathcal{T})} \tag{13}$$

For the wing used in the present design, $A_W = 10$, $E = 1.10$, $\mathcal{T} = 0.25$. The three-dimensional lift-curve slope was calculated to be

$$a = 4.17 \text{ / radian}$$

Ailerons. For the purpose of this preliminary design, the ailerons were sized to occupy the outboard 1/3 of the wingspan and were 1/4 wing chord in depth (Ref 1: 4:6). To assist in overcoming adverse yaw in turns, the ailerons may be rigged differentially. Aileron planform is rectangular with the following dimensions:

Aileron Span	5.0 ft
Aileron Chord	0.75 ft

Gross Surface Area of the Wing. The gross surface area of the wing is the area of the curved surface. The span was computed by laying out a scale drawing of the wing cross-section and measuring the lengths of the top and bottom surfaces with a flexible tape. The results were considered to be as accurate for these purposes as a numerical integration. The results are

Gross area top surface	13,668 in^2 (94.9 ft^2)
Gross area bottom surface	13,068 in^2 (90.7 ft^2)

The areas of the end panels were evaluated by Simpson's
Rule. The cross-sectional area of the wing (one end panel)
is 108.9 in^2.

The gross surface area of the entire wing includes
the top, bottom, and ends, including that area which would
otherwise be removed due to intersection with the fuselage.
The gross surface area is

$$S_{WG} = 26,953 \text{ in}^2 = 187 \text{ ft}^2$$

Wing Placement on Fuselage. A high-wing configuration
was selected. Its effect is to increase static lateral
stability (Ref 11:345, 46). Furthermore, the high wing
can be carried straight through the fuselage without inter-
fering with payload placement.

The aerodynamic center of the wing, located at the
quarter chord subsonically, was placed 79.0 in from the
nose of the aircraft. The highest point of the top surface
was placed tangent to the top of the fuselage. The angle
of incidence was set to zero degrees. Table IV summarizes
the wing and aileron data.

Horizontal Tail

Airfoil Selection. The airfoil selected for the
horizontal tail was the NACA 0009, a 9% thick, symmetrical
section, with the thickest point at 30% of chord. The
cross-section of the NACA 0009 is shown in Figure 6.

Horizontal Tail Size. Corning (Ref 1: 4:38) gives
an approximate method for determining the size of the
horizontal tail:

Table IV

Summary of Wing and Aileron Design Parameters

Section Designation	Clark Y Without Twist, Taper, Sweep, Dihedral or Flaps
Span	30 ft
Chord	3 ft (Constant)
Aspect Ratio	10
Planform Area	90 ft^2
Gross Surface Area	187 ft^2
Lift Coefficient at Stall	1.11
Lift-Curve Slope	4.17 / rad
Placement on Fuselage	High Wing
Aileron Placement	Outboard 1/3 of Span
Aileron Span	5.0 ft
Aileron Chord	0.75 ft
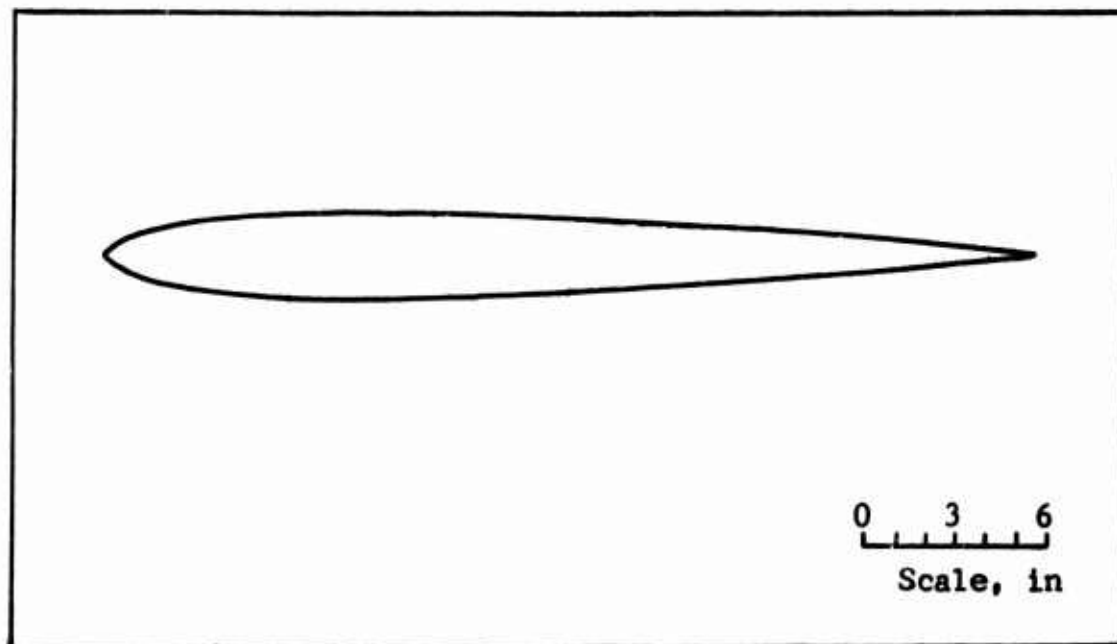
Figure 6.   The NACA 0009

$$S_H = V_H \ \frac{(S_W)(\bar{c})}{l_H} \tag{14}$$

This equation yields a preliminary estimate only, and that size will be used in this report. In practice, the horizontal tail is finally sized during additional cycles of design using a stability and control analysis.

The horizontal tail volume coefficient, V_H, was chosen to be 0.5, as suggested by Professor Larsen. One of the factors which determined the length of the fuselage was the distance between quarter mean aerodynamic chords of wing and horizontal tail. This distance is 100.0 in. The horizontal tail planform area thus became

$$S_H = 16 \ ft^2$$

This area was divided into two rectangular panels, each unswept, of constant chord 2.5 ft and span 3.2 ft. A small

28

amount of additional area was included to shape the inboard
ends of the tail to fit the curve of the fuselage.

The entire horizontal tail assembly is full-flying,
and it is pivoted at the aerodynamic center. The tail was
positioned longitudinally so that the trailing half of the
chord lay aft of the rear end of the fuselage.

Slope of the Lift Curve. The horizontal tail lift-
curve slope was found in the same manner as was the lift-
curve slope of the wing. From NACA Report 669

$$a_o = 6.51 \text{ / radian}$$

For a total tail span of 7.4 ft, chord of 2.5 ft, and $\gamma = 0.09$
(Ref 2:3.17), the three-dimensional lift-curve slope of the
horizontal tail is

$$(C_{L_\alpha})_H = 3.11 \text{ / radian}$$

Gross Surface Area of the Horizontal Tail. The gross
surface area was found by measuring the lengths of top and
bottom surfaces from a scale drawing (see Figure 6). Using
the dimensions given for the lengths of the rectangular
tail panels, the areas of the top and bottom are

Gross area top surface	2332 in^2	(16.2 ft^2)
Gross area bottom surface	2332 in^2	(16.2 ft^2)

The cross-sectional area was evaluated by Simpson's Rule,
and for a single end panel it is 54.7 in^2. Finally, the
gross surface area is

$$S_{HG} = 4882.8 \text{ in}^2 = 33.9 \text{ ft}^2$$

Tail Placement. The horizontal tail was placed on
the fuselage such that its pivot points joined together

would intersect the longitudinal axis of the fuselage. This configuration ensures that, as the glider is flown at increasingly higher angles of attack, the horizontal tail is moved out of the wing wake.

Table V summarizes the data for the horizontal tail.

Vertical Tail

Airfoil Selection. The NACA 0009 was also selected for the vertical tail.

Vertical Tail Size. Corning (Ref 1: 4:38) gives an approximate method for sizing the vertical tail. The limitations are the same as those for Equation (14).

$$S_V = V_V \; \frac{(S_W)(b)}{l_V} \qquad (15)$$

The vertical tail volume coefficient, V_V, was taken as 0.02, as suggested by Professor Larsen. The distance l_V between the quarter mean aerodynamic chords of wing and vertical tail was set at 100.0 in. The planform area of the vertical is

$$S_V = 6.5 \; ft^2$$

The vertical tail is divided into two trapezoidal panels: a fixed vertical fin and a movable flap. The flap chord was selected to be one-third the total local tail chord length. The hingeline was swept 30° in order to allow mounting of the fixed fin completely on the body of the fuselage while simultaneously holding l_V at 100.0 inches. The position of the tail is shown in the fuselage

Table V

Summary of Horizontal Tail Design Parameters

Section Designation	NACA 0009 with Unswept, Rectangular Planform
Volume Coefficient	0.5
Span	8.4 ft
Chord	2.5 ft
Aspect Ratio	3.36
Taper Ratio	1
Planform Area	16 ft^2
Gross Surface Area	33.9 ft^2
Lift-Curve Slope	3.11 / rad
Placement on Fuselage	Full-Flying, Hinged at Longitudinal Axis

configuration, Figure 7.

The height of the vertical tail from the base of the rudder is 3.1 ft. The length of the tip chord is 2.1 ft. The root chord was defined by extending the base of the rudder toward the nose of the glider until it intersected the extension of the leading edge of the vertical fin. The length of the root chord is 3.3 ft. A portion of this chord lies within the fuselage. The actual planform area exposed to the airstream is slightly in excess of the amount required by Equation (15). The actual area is

$$S_V = 7.4 \text{ ft}^2$$

The length of the mean aerodynamic chord was computed as follows:

$$\bar{c}_V = \frac{2}{3} \left[c_r + c_t - \frac{c_r c_t}{c_r + c_t} \right] \tag{16}$$

so that

$$\bar{c}_V = 2.75 \text{ ft}$$

The taper ratio is defined as

$$\lambda = \frac{\text{Tip Chord}}{\text{Root Chord}} \tag{17}$$

For the vertical tail the taper ratio is

$$\lambda = 0.637$$

The aspect ratio is a corrected, or effective, aspect ratio based on the tail surface area, including that area concealed by the fuselage. The effective aspect ratio is given by

$$A_{eff_V} = (1.5) \frac{b^2}{S_V} \tag{18}$$

Figure 7

Fuselage Longitudinal Section

Scale, ft
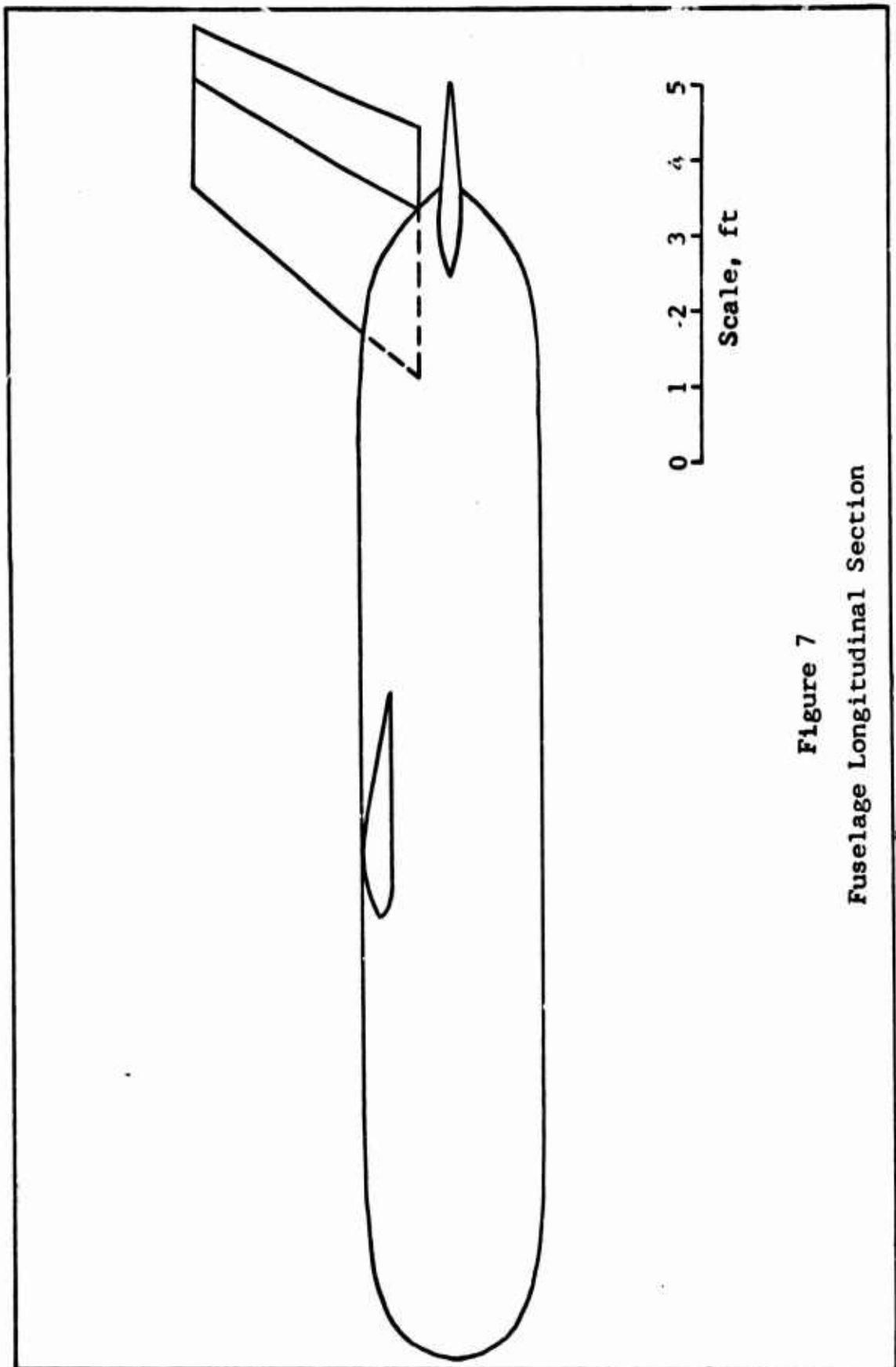
which, for the vertical tail, is

$$A_{eff_V} = 1.72$$

Slope of the Lift Curve. The vertical tail is both tapered and swept, and there is an endplate effect due to the presence of the fuselage. Etkin (Ref 6:446, 449, 455) gives a method for finding the lift-curve slope under such circumstances. Entering arguments for the Etkin table are quarter-chord sweep (37°), taper ratio, and the parameter ($\beta A_V / \kappa$). The endplate effect multiplies the three-dimensional lift-curve slope by 2.9. The three-dimensional lift-curve slope of the vertical tail is

$$(C_{L_\alpha})_V = 4.64 / \text{radian}$$

Gross Surface Area of the Vertical Tail. The gross surface area of the vertical tail was found by laying out scale drawings of tip and root airfoils, measuring the lengths of the top and bottom of each airfoil, and finding the resultant areas of the trapezoids using the lengths of root and tip airfoils as bases. These areas are:

Total right and left lateral surfaces	2514 in^2 (17.5 ft^2)
Top face	38.6 in^2 (0.27 ft^2)
Bottom face	95.3 in^2 (0.66 ft^2)

The gross surface area is

$$S_{VG} = 2648 \text{ in}^2 = 18.4 \text{ ft}^2$$

Table VI summarizes the data for the vertical tail.

Combined Fuselage. Figure 7 shows a longitudinal section of the fuselage configuration.

Table VI

Summary of Vertical Tail Design Parameters

Section Designation	NACA 0009 with Swept, Trapezoidal Planform
Volume Coefficient	0.02
Height from Base of Rudder	3.1 ft
Height from Longitudinal Axis of Fuselage	3.5 ft
Length of Root Chord	3.3 ft
Length of Tip Chord	2.1 ft
Length of Mean Aerodynamic Chord	2.75 ft
Length of Any Rudder Chord	1/3 Length of Total Tail Chord at that Station
Sweep Angle of Hingeline	30 deg
Sweep Angle of Leading Edge	41 deg
Sweep Angle of Quarter Chord	37 deg
Effective Aspect Ratio	1.72
Taper Ratio	0.647
Exposed Planform Area	7.4 ft^2
Gross Surface Area	18.4 ft^2
Lift-Curve Slope	4.64 / rad

Free-Flight Vehicle Weight and Balance

The combined vehicle weight and balance was analyzed assuming the glider to be a free-flight (i.e., untowed) vehicle. It has a fixed center of gravity throughout its mission profile, although variable towline tension replaces center of gravity travel. The effect of the towline will be considered in Section VIII.

To be longitudinally stable, the aircraft center of gravity must be ahead of the stick-fixed neutral point. The more longitudinally stable the aircraft, the more control force and displacement needed to effect pitch changes (Ref 6:78).

Table VII presents the weight and balance data. The center of gravity of each item of payload was assumed to be at the geometric center of that item. Moment arms were measured in inches, positive toward the tail, using the nose as zero datum.

The longitudinal position of the center of gravity is given by Equation (19).

$$x_c = \frac{\text{Total Moment}}{\text{Total Weight}} \tag{19}$$

The center of gravity is at 76.7 in. Not included in the computations were a wheel, estimated weight five pounds, and a tow hitch, estimated weight less than one pound. Both of these items were placed respectively below and above the center of gravity after determination, and thus they do not affect its position.

Table VII

Weight and Balance Data

Component	Weight, lb	Dist from Nose, in	Moment, lb-in
Fuselage, Empty	70.0	93.0	6510.0
Wing	70.0	83.9	5873.0
Horizontal Tail	8.0	186.0	1488.0
Vertical Tail	5.0	186.0	930.0
LLLTV Camera	45.0	13.5	607.5
Camera Electronics	31.0	38.5	1193.5
Aircraft Battery	80.0	59.0	4720.0
Power Supply	70.4	79.5	5596.8
Junction Box	29.9	106.0	3169.4
Operator Electronics	23.0	132.5	3047.5
Transmitter	2.2	132.5	291.5
	436.5		33427.2

VI. Vehicle Performance in Free Flight

This section analyzes the performance of the glider as a free-flight vehicle. The following performance parameters will be analyzed:

1. Lift-drag relationship (Drag Polar).

2. Glide ratio for various angles of attack.

3. Stall speed for various bank angles.

4. Radius of turn at various bank angles.

Combined Vehicle Lift-Drag Relationship

The vehicle drag coefficient may be expressed as follows:

$$C_D = C_{D_{pe}} + \frac{1}{\pi A_W e} \; C_L^2 \tag{20}$$

where $C_{D_{pe}}$ is the equivalent parasite drag coefficient. $C_{D_{pe}}$ is referred to wing planform area and is multiplied by 1.1 to account for the effects of pressure drag. The pressure drag in the low-speed flight regime with which this design is concerned accounts for about 10% of the skin friction (parasite) drag.

Wetted Area Method for Computation of Parasite Drag

The parasite drag term is expressed as follows:

$$C_{D_{pe}} = \frac{K \sum c_{f_i} S_{wet_i}}{S_W} \tag{21}$$

where K is between 1.1 and 1.2. The summation is taken

over each of the individual parts of the airframe which are
exposed to the flow of air in flight. The skin friction
coefficient, c_f, is presented by Corning (Ref 1: 2:38, 39)
as a function of Reynolds Number and Mach Number. The
Reynolds Numbers were evaluated at the trailing edge of
the appropriate aircraft component. Turbulent skin fric-
tion coefficients were used for the preliminary estimate in
this design. Future cycles of design would consider the
actual surface roughness in a more accurate estimate of the
parasite drag coefficient. Schlichting (Ref 13:552), for
example, presents charts for computing such skin friction
coefficients.

The wetted area of an aircraft component is that por-
tion of the area which is actually exposed to the airstream.
Wetted area is computed by subtracting from the gross surface
area the individual area losses due to intersection with
other parts of the structure. For example, the wetted
area of the wing is the gross surface area, including end
panels, minus the amount of area removed due to intersection
with the fuselage. Following are the wetted areas for each
component of the aircraft structure. Included are estimates
for a tow hitch (4 in^2) and a blade-type antenna (20 in^2).
Details of the computation of the various areas are included
in Appendix C.

Wetted Area of the Fuselage.

$$S_{wet_{fs}} = S_{fsG} - \Delta S_{wet_W} - \Delta S_{wet_V} - \Delta S_{wet_H} \qquad (22)$$

$$- \Delta S_{wet_{WL}} - \Delta S_{wet_{TH}} - \Delta S_{wet_{ANT}}$$

$$S_{wet_{fs}} = 14,727.6 \text{ in}^2 = 102.3 \text{ ft}^2$$

Wetted Area of the Wing.

$$S_{wet_W} = S_{WG} - \Delta S_{wet_{fs}} \qquad (23)$$

$$S_{wet_W} = 25,298.2 \text{ in}^2 = 175.5 \text{ ft}^2$$

Wetted Area of the Horizontal Tail.

$$S_{wet_H} = S_{HG} - \Delta S_{wet_{fs}} \qquad (24)$$

$$S_{wet_H} = 4828.1 \text{ in}^2 = 33.5 \text{ ft}^2$$

Wetted Area of the Vertical Tail.

$$S_{wet_V} = S_{VG} - \Delta S_{wet_{fs}} = 2317.8 \text{ in}^8 \qquad (25)$$

Wetted Area of the Wheel. The wheel is estimated to be 8 in in diameter and 2 in thick. One-half the wheel is exposed.

$$S_{wet_{WL}} = \tfrac{1}{2} S_{WLG} \qquad (26)$$

$$S_{wet_{WL}} = 75.5 \text{ in}^2 = 0.523 \text{ ft}^2$$

Wetted Area of the Tow Hitch. The wetted area of the tow hitch was assumed to be 4 in^2.

$$S_{wet_{TH}} = 4 \text{ in}^2$$

Wetted Area of the Antenna. The wetted area of the antenna was assumed to be 20 in^2.

$$S_{wet_{ANT}} = 20 \text{ in}^2$$

Reynolds Number Computation. The Reynolds Number based on length is given by Equation (27).

$$R = \frac{\rho V l}{\mu} \qquad (27)$$

These numbers were evaluated for mean sea level density, viscosity, and aircraft stall speed. These conditions yield the most conservative values of skin friction coefficient. Under these conditions, the Reynolds Number at any length, l, is given by

$$R = 3.878 \times 10^5 \, l \qquad (28)$$

where l is in feet. Once the Reynolds Numbers were determined, the corresponding skin friction coefficients were found from Corning (Ref 1: 2:38, 39). They are listed in Table VIII. Finally, from Equation (21), the value for the parasite drag coefficient is

$$C_{D_{pe}} = 0.015972$$

Induced Drag Coefficient

The second term in Equation (20) represents the induced drag coefficient, or the coefficient of drag due to lift. The factor e is an empirical one and it is taken as 0.8 for this aircraft. The factor accounts for the following:

1. Increase in drag due to non-elliptical load distribution across the wingspan.

2. Increase in trim drag.

3. Increase in drag attributable to angle of attack on all aircraft components.

Generally always less than unity, e represents an increase

in drag and is called the "airplane efficiency factor"
(Ref 1: 7:12). The value of the induced drag coefficient
is

$$C_{D_i} = 0.0398 \, C_L^2$$

The Drag Polar

The drag polar for the aircraft is the sum of parasite
and induced drags. The drag polar is

$$C_D = 0.015972 + 0.0398 \, C_L^2 \tag{29}$$

and it is plotted in Figure 8. Beyond 90% of $C_{L_{max}}$ the
curve becomes nonlinear and was approximated by a parabola.
The parabolic portion of the curve was plotted using $0.9C_{L_{max}}$
as an origin and taking for the equation of the curve

$$\Delta C_{D_p} = K \, x^2 \tag{30}$$

where x is a nondimensional variable defined as follows:

$$x = \frac{C_L - 0.9 \, C_{L_{max}}}{C_{L_{max}} - 0.9 \, C_{L_{max}}}$$

The value of ΔC_{D_p} was taken as being 0.3. From Equation
(30), K = 0.3 at x = 1. Beyond the linear range the curve
is, therefore, approximated as

$$C_D = C_{D_{pe}} + \frac{1}{\pi A_W e} \, C_L^2 + 0.3 \, x^2 \tag{31}$$

Glide Ratio

For a glider in free flight, the lift-to-drag ratio,
or glide ratio, is uniquely determined by angle of attack.
For any angle of attack, the glide ratio may be found by
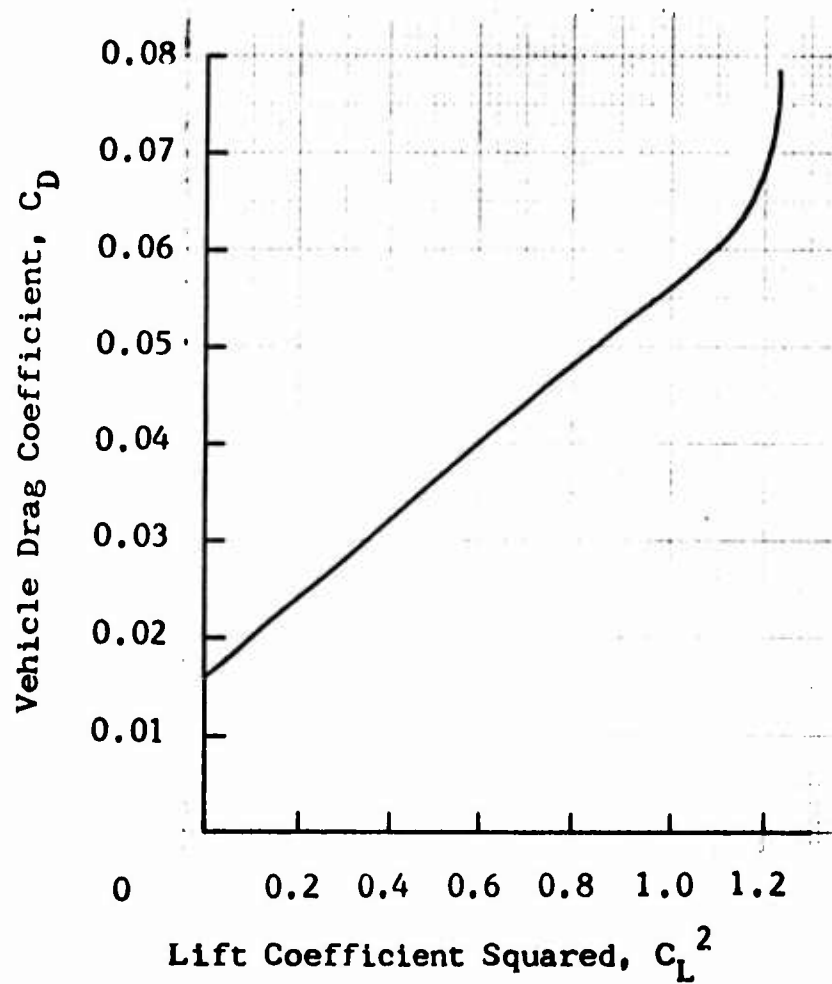
Figure 8

Vehicle Drag Polar

Table VIII

Skin Friction Coefficients

	R	c_f
Fuselage	6.01×10^6	0.0032
Wing	1.16×10^6	0.0043
Horizontal Tail	1.00×10^6	0.0044
Vertical Tail	9.68×10^5	0.0044
Wheel	2.59×10^5	0.0058
Tow Hitch	6.59×10^4	0.0054
Antenna	1.28×10^5	0.0068

using the data in Figure 8, since

$$\frac{L}{D} = \frac{\frac{1}{2} \rho V^2 S_W C_L}{\frac{1}{2} \rho V^2 S_W C_D} = \frac{C_L}{C_D} \tag{32}$$

At any given lift coefficient

$$C_L = C_{L_\alpha} (\alpha - \alpha_{ZL}) \tag{33}$$

In Equation (33) C_{L_α} is the lift-curve slope for the aircraft as a whole. It was taken as 95% of the lift-curve slope for the wing alone.

Figure 9 shows the change in L/D ratio versus angle of attack through the linear range. The best glide ratio achieveable is 19.8 occurring at an angle of attack of 9°.

Stall Speed

Equation (5) related stall speed to wing loading. Under mean sea level conditions the straight-ahead stall speed is
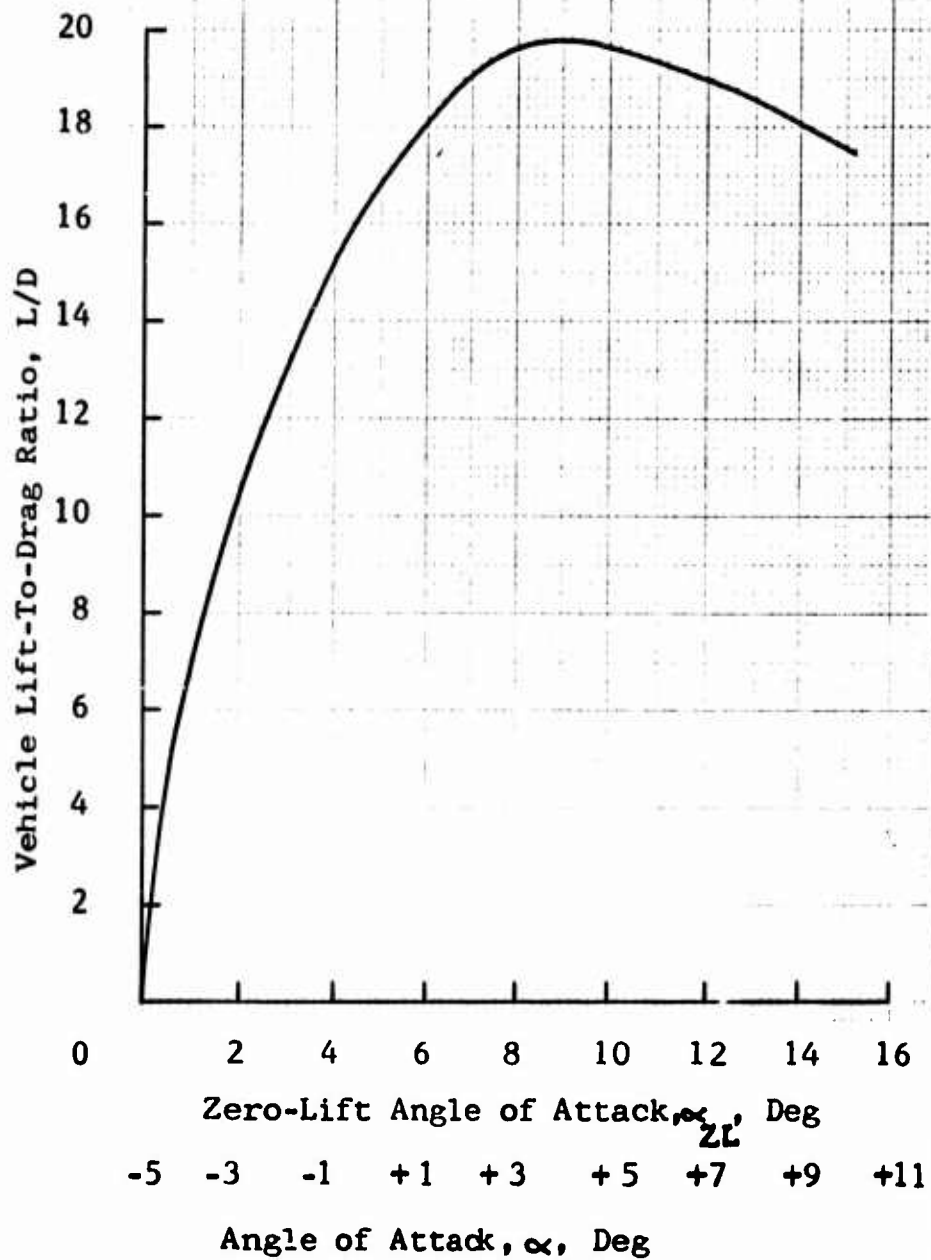
Figure 9

Vehicle Lift-to-Drag Ratio
for the Linear Region

60.6 ft/sec or 35.8 knots. The stall speed increases when
the glider is in turning flight. Stall speed can be re-
lated to load factor which is, in turn, a function of the
bank angle for a coordinated turn. The relation between
straight-ahead stall speed and stall speed in a coordinated,
level turn is given by Equation (34).

$$V'_S = V_S \sqrt{n} \tag{34}$$

The load factor in a coordinated, level turn is numerically
equal to the secant of the bank angle (Ref 3:IV-4). Table IX
presents the stall speeds in feet per second and in knots
for selected bank angles. This table has several limitations.
A glider loses altitude in a turn, and this has been neglect-
ed in the results of Table IX. Sink rate increases with
bank angle.

It is improbable that the glider will make use of turns
of bank angle greater than 60°. To obtain the stall at
large bank angles requires relatively high airspeed. Obtain-
ing high airspeed requires the application of power. A
glider makes up for this lack of power by diving. Steeply
banked turns are flown in descending spirals. Such perfor-
mance is inapplicable to the present mission. Other limits
on the bank angle may be imposed by structural limitations
because of load factors.

Turn Radius

The radius of turn may be obtained as a function of
the airspeed and load factor. The relation is (Ref 3:IV-5):

Table IX

Stall Speeds and Load Factors for Selected Bank
Angles for Coordinated, Level Turns
at Mean Sea Level

Bank Angle, deg	Load Factor, g's	Stall Speed, ft/sec	Stall Speed, Knots
0	1.00	60.6	35.8
10	1.02	61.1	36.2
20	1.06	62.5	37.0
30	1.15	65.2	38.5
40	1.31	69.2	41.1
50	1.56	75.6	44.7
60	2.00	85.8	50.8
(70)	(2.92)	(103.5)	(63.3)
(80)	(5.76)	(145.5)	(85.9)

Stall Speed doubles at 75 degrees of bank

$$R = \frac{V^2}{g\sqrt{n^2 - 1}} \qquad (35)$$

where R is the radius of a level turn. The turn is flown at $C_{L_{max}}$, just on the boundary of the stall. Table X shows the radius of turn in feet for a level turn at selected bank angles.

The results of Table X must also be interpreted with caution. Several factors limit the turn radius. The radius given by Equation (35) is that of a g-limited turn. Aircraft structural limitations may limit the load factor which can be imposed, requiring a less tight turn. The effect of the tow cable on turning performance is not known. The tow cable provides thrust and a component of the lift. A flight test would be required to determine how the turn rates of glider and towplane would have to be matched. It is anticipated, however, from the point of view of the towplane-glider combination, that the glider would be flown in shallow turns or suspended in Long-Line-Loiter.

Table X

Radius of a Coordinated, Level Turn at $C_{L_{max}}$
for Selected Bank Angles at Mean Sea Level

Bank Angle, deg	True Airspeed, knots	Turn Radius, ft
10	36.2	579
20	37.0	344
30	38.5	231
40	41.1	176
50	44.7	148
60	50.8	132
(70)	(63.3)	(122)
(80)	(85.9)	(116)

VII. Static Stability and Control of the
Glider in Free Flight

This section will include a discussion of the static stability of the vehicle in free flight, a computation of the static margin, and a computation of the rudder power. The effect of the towline will be considered in the next section.

Static stability is concerned with the direction of the moment created by a slight perturbation from the equilibrium flight path. At some given flight condition, the aircraft is said to be statically stable if a slight attitude perturbation creates a moment which tends to restore the vehicle to the trimmed condition (Ref 3:VIII-1).

The glider in free flight will be statically stable if (Ref 4:1)

C_{m_α} (Longitudinal stability derivative) < 0

C_{l_β} (Lateral stability derivative) < 0

C_{n_β} (Directional stability derivative) > 0

Static Longitudinal Stability

By way of simplification for this preliminary design, it will be assumed that

1. The aircraft drag force, acting through the aerodynamic center of the wing-body combination, does not contribute to C_{m_α}.

2. The aerodynamic center of the wing-body combination

50

is at the same longitudinal position as the quarter-chord of the wing alone. Under these conditions the static longitudinal stability derivative is given by (Ref 4:VIII-9)

$$C_{m_\alpha} = (C_{L_\alpha})_{WB} \bar{x} - \left(1 - \frac{\partial \epsilon}{\partial \alpha}\right) \eta_H V_H (C_{L_\alpha})_H \qquad (36)$$

The parameter $\partial \epsilon / \partial \alpha$ is the partial derivative of the downwash angle at the tail with respect to angle of attack. It is a function of the location of the tail behind the wing trailing edge (Ref 4:2). The non-dimensional distance $\bar{x}$ is a negative quantity as long as the wing-body aerodynamic center is behind the aircraft center of gravity. The tail efficiency factor, η_H, is assumed to be unity. From Corning (Ref 1: 9:34, Fig. 9:19, 9:20), $\partial \epsilon / \partial \alpha = 0.258$. The lift-curve slope for the horizontal tail is 3.11 / radian. The horizontal tail volume coefficient is 0.5. Using a lift-curve slope of the wing-body combination of 3.96 / radian the value of the longitudinal stability derivative becomes

$$C_{m_\alpha} = -1.405 \text{ / radian}$$

The glider in free flight possesses static longitudinal stability.

Static Lateral Stability

The static lateral stability (or dihedral) derivative is influenced by three factors: the wing dihedral and sweep, the vertical tail, and the wing-fuselage interaction. The stability derivative is treated as a linear combination of the three factors (Ref 4:4).

Effect of Wing Dihedral and Sweep. The wing has
neither geometric dihedral nor sweep. The contribution
from this source is zero (Ref 4:5).

Effect of Vertical Tail. The effect of a conventional
vertical tail derives from the force on the tail which is
generated as the aircraft sideslips. A restoring moment
is provided by the tail which acts through a moment arm to
the center of gravity. This contribution is stabilizing.
It may be expressed as follows:

$$(C_{l_\beta})_V = -(C_{L_\alpha})_V \left(1 + \frac{\partial \sigma}{\partial \beta}\right)\frac{q_V}{q} \frac{S_V}{S_W} \frac{z_V}{b} \qquad (37)$$

The parameter $\left(1 + \frac{\partial \sigma}{\partial \beta}\right)\frac{q_V}{q}$ is difficult to determine, but

an approximation is given as

$$\left(1 + \frac{\partial \sigma}{\partial \beta}\right)\frac{q_V}{q} = 0.724 + \frac{3.06 \frac{S_V}{S_W}}{1 + \cos \Lambda_{c/4}} + 0.4 \frac{z_W}{d} + 0.009 A_W \qquad (38)$$

The vertical tail area to be used in Equation (38) is the
vertical tail area with the root chord extended downward to
the fuselage centerline (Ref 4:7). The value of this con-
tribution is -0.0271 / radian.

Effect of Wing-Fuselage Interaction. If the wing is
placed high on the fuselage the interference effect between
the wing and fuselage acts to increase the lateral stability
by increasing effective dihedral. This effect can be esti-
mated as follows (Ref 11:346):

$$(C_{l_\beta})_W = -0.0344 / radian$$

By adding the three contributions to the lateral
stability, the value of the static lateral stability
derivative for the aircraft becomes

$$C_{l_\beta} = -0.0615 \text{ / radian}$$

Because this value is negative the glider exhibits static
lateral stability.

Static Directional Stability

The requirement for directional (or weathercock)
stability derives from the sideslip condition. When the
glider is at a sideslip angle β relative to the flight
path, a yawing moment must be produced which tends to re-
store the glider to symmetric flight. A right slip is
defined as positive, and it results in a positive yawing
moment. For static directional stability the directional
stability derivative must be positive (Ref 6:79, 82).

The directional stability derivative is influenced
by three factors: the wing, the fuselage, and the vertical
tail.

Effect of the Wing. The wing contribution is due to
the asymmetrical drag and lift distributions on the different
wing panels undergoing sideslip. This contribution is

$$(C_{n_\beta})_W = C_L^2 \left[\frac{1}{4\pi A_W} - \frac{\tan \Lambda_{c/4}}{\pi A_W (A_W + 4\cos \Lambda_{c/4})} (\cos \Lambda_{c/4} - \frac{A_W}{2} - \frac{A_W^2}{8 \cos \Lambda_{c/4}} + \frac{6x}{\bar{c}} \frac{\sin \Lambda_{c/4}}{A_W}) \right] \text{ /radian}$$

(39)

Since the quarter-chord sweep is zero, Equation (39) reduces

to

$$(C_{n_\beta})_W = C_L^2 \; \frac{1}{4 \pi A_W} \; / \text{ radian} \qquad (40)$$

which is

$$(C_{n_\beta})_W = 0.00795 \, C_L^2 \; / \text{ radian}$$

Effect of the Fuselage. The fuselage is usually de-stabilizing since the vehicle center of pressure is usually ahead of the vehicle center of gravity. The effect of the fuselage was estimated as follows (Ref 4:9):

$$(C_{n_\beta})_{fs} = -1.3 \; \frac{V_F}{S_W b} \; \frac{h}{w} \; / \text{ radian} \qquad (41)$$

The magnitude of this contribution is

$$(C_{n_\beta})_{fs} = -0.0286 \; / \text{ radian}$$

Effect of the Vertical Tail. The conventional tail is stabilizing as long as the tail is behind the aircraft center of gravity. The effect of the vertical tail was estimated as follows (Ref 4:9):

$$(C_{n_\beta})_V = (C_{L_\alpha})_V \; (1 + \frac{\partial \sigma}{\partial \beta}) \; \frac{q_V}{q} \, V_V \qquad (42)$$

The magnitude of this contribution is

$$(C_{n_\beta})_V = 0.1042 \; / \text{ radian}$$

The directional stability derivative is the sum of each of the three above contributions. It is

$$C_{n_\beta} = 0.0756 + 0.00795 \, C_L^2 \; / \text{ radian}$$

Since C_L^2 is positive for all values of C_L, the entire

stability derivative is positive, and the glider exhibits static directional stability.

Static Margin

The static margin is a measure of the degree of static longitudinal stability. The static margin is the non-dimensional distance (with respect to mean aerodynamic chord) of the center of gravity ahead of the stick-fixed neutral point. The stick-fixed neutral point is the center of gravity location for which the static longitudinal stability derivative is zero (Ref 3:VIII-10). Thus, from Equation (36),

$$(C_{l_\alpha})_{WB} \, \bar{x}_n - (1 - \frac{\partial \epsilon}{\partial \alpha}) \, \eta_H V_H (C_{L_\alpha})_H = 0 \qquad (43)$$

The distance between the center of mass and the aerodynamic center of the horizontal tail depends on the value of $\bar{x}_n$. Using Dittrich's method (Ref 3:VIII-10, 11), the value of $\bar{x}_n$ is given by

$$\bar{x}_n = \frac{(1 - \frac{\partial \epsilon}{\partial \alpha}) \, \eta_H \, \frac{S_H l_{ac}}{S_W \bar{c}} \, \frac{(C_{L_\alpha})_H}{(C_{L_\alpha})_{WB}}}{1 + (1 - \frac{\partial \epsilon}{\partial \alpha}) \eta_H \, \frac{S_H}{S_W} \, \frac{(C_{L_\alpha})_H}{(C_{L_\alpha})_{WB}}} \qquad (44)$$

or, $\bar{x}_n = 0.26$

This quantity represents the non-dimensional distance of the wing-body aerodynamic center ahead of the aircraft center of gravity. The static margin is given by

$$SM = \bar{x}_n - \bar{x} \qquad (45)$$

giving a value for the static margin of

$$SM = +0.196$$

A positive value of static margin indicates static longitudinal stability (Ref 3:VIII-12). In the free-flight condition, the glider has a high degree of static stability in pitch; however, the effect of the towline is to render the aircraft less stable.

Rudder Power

In most flight conditions the sideslip angle is maintained at zero. Yawing moments will act on the glider when it is flown in trail other than directly behind the towplane because of the force of the tow cable. Knowing how effective the rudder is in maintaining a given sideslip angle is an important guage of the glider's performance. The rudder deflection necessary to hold a given sideslip angle, wings level, is determined as a free-flight phenomenon. The relationship for steady motion is (Ref 6:84)

$$\frac{\beta}{\delta_r} = - \frac{C_{n_\delta}}{C_{n_\beta}} \qquad (46)$$

where C_{n_δ} is the rate of change of yawing moment with rudder deflection:

$$C_{n_\delta} = -a_r V_V \left(\frac{V_F}{V}\right)^2 \qquad (47)$$

When the vertical tail is not in a propeller slipstream, the velocity ratio (V_F/V) is unity (Ref 6:83). The value

of a_r is found by the method presented by Etkin (Ref 6:456-461, Figs B.2-1, B.2-2, and B.2-4). The value is

$$a_r = 3.33 \text{ / radian}$$

Equation (46) was solved for the relationship between sideslip angle and rudder deflection angle to yield

$$\beta = 0.639 \ \delta_r$$

To hold a sideslip angle of 10°, for example, requires a rudder deflection angle of $15\frac{1}{2}^o$.

Summary of the Stability and Control Parameters

Table XI summarizes the static stability derivatives, and control parameters for the aircraft.

Table XI

Summary of Static Stability and Control Parameters

Stability Derivative	Requirement	Predicted Value
Longitudinal C_{m_α}	< 0	-1.405 / rad
Lateral C_{l_β}	< 0	-0.615 / rad
Directional C_{n_β}	> 0	$0.0756 + 0.00795\, C_L^2$ / rad

The Static Margin is $+0.196$ indicating a high degree of Longitudinal Stability

For a rudder deflection of $15\frac{1}{2}$ deg the aircraft, in free flight, will maintain a sideslip angle of 10 deg.

VIII. The Glider in Towed Flight

To satisfy the design requirement given on Page 6, the glider must be flyable while being towed at high and low speeds. The tow cable was attached to the vehicle on the top surface of the fuselage directly above the center of gravity. The equations of static equilibrium are satisfied for towed flight at high speed within the limits of motion for elevator and rudder, as will be shown in this section.

Figure 10 shows a schematic of the longitudinal section. For equilibrium flight at angle of attack, α, the equations of static equilibrium are:

(ΣF_x):
$$- T \sin \phi - L \cos \alpha - D \sin \alpha - L_H \cos(\alpha - \epsilon)$$
$$- D_H \sin(\alpha - \epsilon) + W = 0 \qquad (48)$$

(ΣF_y):
$$T \cos \phi + L \sin \alpha - D \cos \alpha + L_H \sin(\alpha - \epsilon)$$
$$- D_H \cos(\alpha - \epsilon) = 0 \qquad (49)$$

(ΣM_{cg}):
$$(\hat{i} x_R - \hat{k} z_R) \times (\hat{i} T \cos \phi - \hat{k} T \sin \phi)$$
$$+ (- \hat{i} x_{ac} - \hat{k} z_{ac}) \times \left[\hat{i} (L \sin \alpha - D \cos \alpha) \right.$$
$$+ \hat{k} (-L \cos \alpha - D \sin \alpha) \Big]$$
$$+ (- \hat{i} l_{HC}) \times \left[\hat{i} (L_H \sin(\alpha - \epsilon) - D_H \cos(\alpha - \epsilon)) \right.$$
$$+ \hat{k} (-L_H \cos(\alpha - \epsilon) - D_H \sin(\alpha - \epsilon)) \Big]$$
$$+ \hat{j} M_{ac_W} + \hat{j} M_{ac_H} = 0 \qquad (50)$$

Figure 10

Schematic of Longitudinal Section
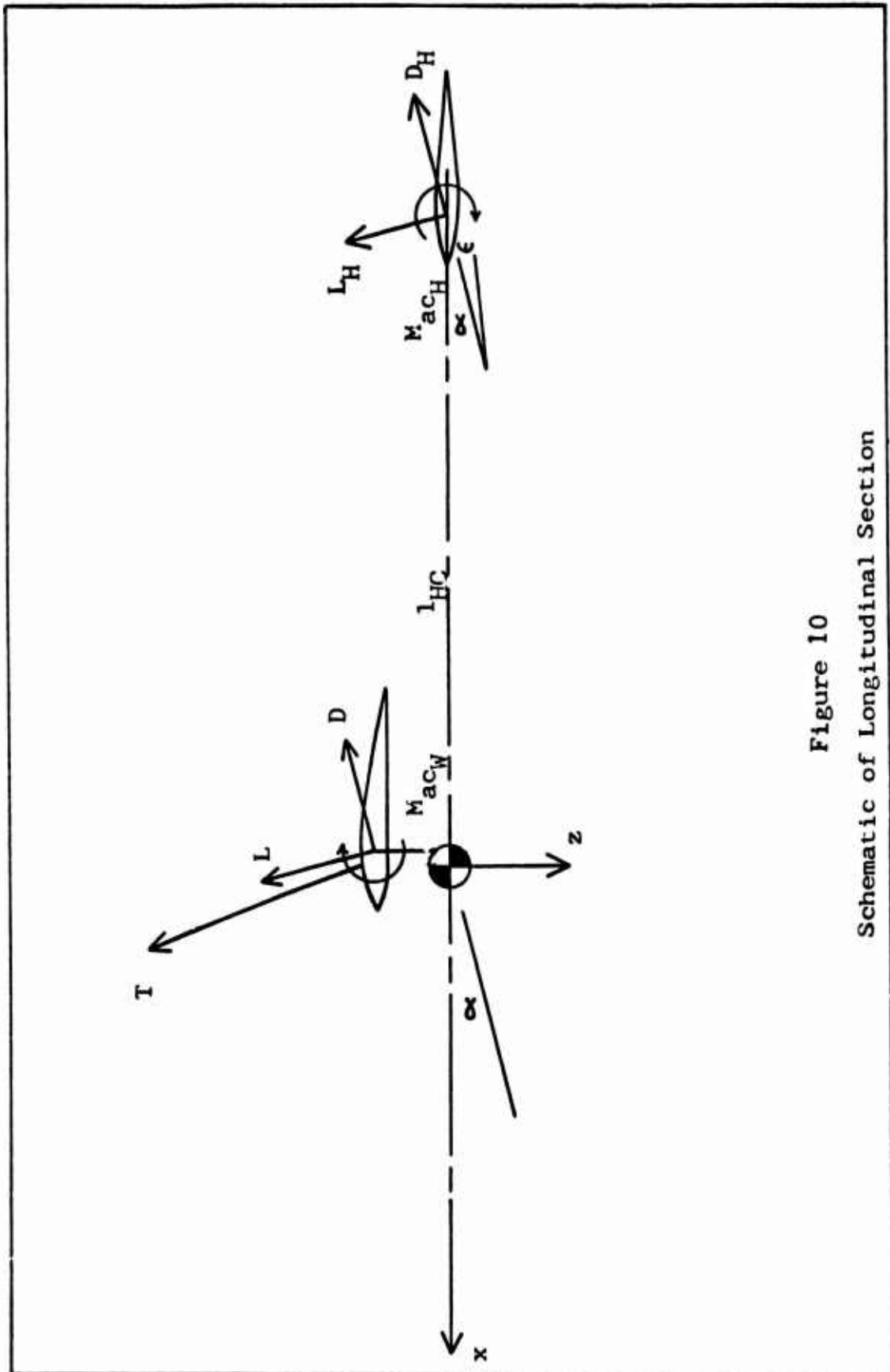
Attaching the tow cable above the aircraft center of gravity allows the glider to hang horizontally while suspended in Long-Line-Loiter. The slewable mirror does not require any additional range of movement between trail and loiter. A horizontal attitude will aid recovery to towed flight. Additionally, this tow cable attachment position must allow the glider to be towed in trail at 150 knots, 800 feet to the side of the towplane and 3,000 feet below. The existing rudder and elevator sizes were found to be adequate to permit both loiter and trail.

To solve the equations of equilibrium, the following simplifications were made:

1. The glider was in equilibrium flight; therefore, the horizontal component of cable tension was equal to the drag.

2. The tow cable met the tow hitch at an angle of 70 deg with respect to the horizontal.

3. The downwash velocity was neglected. The angle of attack of the horizontal tail was measured with respect to the free stream velocity.

The zero-lift angle of attack of the Clark Y is -5°. At an airspeed of 150 knots the wing angle of attack is -4°, allowing small angle assumptions to be applied. The angle of the tow cable was estimated from prior flight tests performed on other drones by personnel of the 6570th Aerospace Medical Research Laboratory. Properties of the atmosphere were taken at 5,000 feet, mean sea level.

61

Equations (48), (49), and (50) include four unknowns:
L, D, L_H, and D_H. One unknown was eliminated by finding the
L/D ratio from Figure 9 and using it as an approximation to
the L/D ratio of the wing alone. This ratio is 7 for an
angle of attack of -4°. L was eliminated from the equations.
The airfoil moments were calculated to be M_{ac_W} = -1249 lbf-ft
(nose down) and M_{ac_H} = 0 (Ref 9:9, 15).

The simplified set of equations with all constants
moved to the righthand side is as follows:

$$- 6.93 \ D - \qquad L_H + 0.07 \ D_H = -442.5 + \ 0.94 \ T \quad (51)$$
$$- 1.49 \ D - 0.07 \ L_H - \qquad D_H = \qquad - \ 0.34 \ T \quad (52)$$
$$0.142 \ D - 8.53 \ L_H + 0.597 \ D_H = \ 1249 \ + 0.396 \ T \quad (53)$$

Applying Cramer's Rule permits solution for the value of
lift of the horizontal tail as a function of cable tension:

$$L_H = \frac{-8448 - 0.667 \ T}{59.6} \qquad (54)$$

Equation (54) shows that the effect of cable tension on the
lift required of the horizontal tail is very small. The
nose-down pitching moment of the wing accounts for nearly
all the force the horizontal tail must balance. The negative
value of L_H indicates that the lift acts in the direction
opposite to that assumed in Figure 10.

To determine towline tension, the vehicle was assumed
to be flying close enough to the zero-lift angle attack that
the zero-lift drag coefficient could be used to evaluate
the aircraft drag. At 150 knots the aircraft drag is 94.8 lbf.

This requires a tow cable tension of 275 lbf. From Equation (54) the lift to be supplied by the tail was computed to be 146.4 lbf. To provide this lift, the horizontal tail must be at an angle of attack of -2.6 degrees. This is well within the capabilities of the movement of the tail.

Placing the tow cable directly above the center of gravity has very little effect on the moments exerted about the center of gravity because of the short moment arms.

When the glider is displaced 800 feet to the side of the towplane and 3,000 feet below, the towline force resolves as follows:

1. A rolling moment which acts inward.

2. A towing force which acts forward.

3. A lift force which acts upward.

No yawing moment acts about the center of gravity. No additional rudder is needed to counteract the towing force.

The brief analysis of this section has demonstrated that, with tow point selected for the low-speed region of the flight envelope, sufficient control power exists to allow the glider to be flown in the high-speed region. A more thorough analysis will require flight test. To counteract the rolling moment, for example, will place a sizing requirement on the ailerons.

IX. Design Summary

This section will discuss how well the final design has met the original specification as stated on Page 6.

1. The vehicle is towable by a C-130 on a line 5,000 feet long. It is manuverable by remote control.

2. With controls sized as given in Section V, the vehicle is maneuverable 800 feet to either side of the towplane while flying in trail 3,000 feet below the altitude of the tow aircraft.

3. The glider is not capable of controlled flight below an airspeed of 35.8 knots, the stright-ahead stall speed.

4. The glider will enter Long-Line-Loiter when the towline stalls. The ground tract and height variation followed after stall have not been determined and will require flight test.

5. No particular altitude restrictions have been placed on the vehicle. It can be flown from 25 feet above ground level (in Long-Line-Loiter) to 5,000 feet above ground level (full-speed trail).

Table XII presents a general summary of the vehicle size and performance parameters. Figure 11 shows the top and front views of the glider. Figures 7 and 11 together constitute a three-view of the glider.

Table XII

Summary of Vehicle Design Features

Design Objective	A Towed Glider to Provide Covert Low-Level, Low- and High-Speed Photoreconnaissance
Payload	Low-Light-Level TV
Payload Weight	282.3 lb
Vehicle Gross Weight	442.5 lb
Wing Span	30 ft
Vehicle Length	17.7 ft
Height from Longitudinal Axis to Top of Vertical Tail	3.5 ft
Wing Section	Clark Y
Wing Chord	3 ft
Vertical, Horizontal Tail Section	NACA 0009
Horizontal Tail Span	8.4 ft
Horizontal Tail Chord	2.5 ft
Vertical Tail Mean Aerodynamic Chord	2.75 ft
Straight-Ahead Stall Speed, Free Flight	35.8 knots
Stall Speed in $60°$ Bank, Coordinated Turn, Free Flight	50.8 knots
Best Glide Ratio, Free Flight	19.8

Figure 11

Top and Rear Views
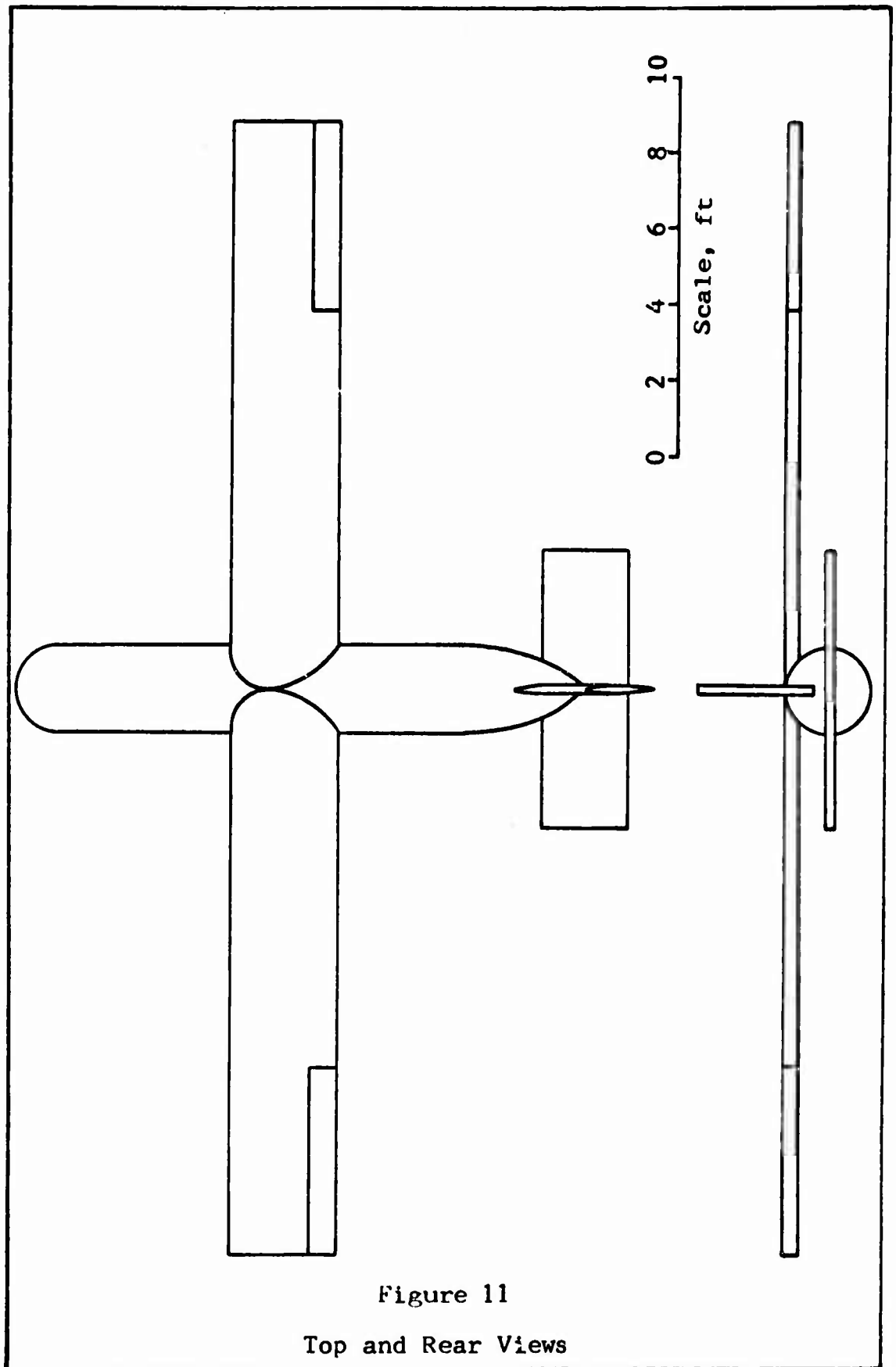
X. Recommendations for Further Study

Structures

The structural problem has been ignored entirely; however, the use of polyurethane foam for interior construction has been suggested. The arrangement of interior structure is still to be determined.

The present design is characteristic of a low-speed glider. While in high-speed trail, the wing is flying nearly at the zero-lift angle of attack. The wing lift coefficient is nearly zero. Should the glider be flown in this configuration through a vertically-upward gust, the wing lift coefficient would be raised to a high value almost instantaneously. If the gust is sufficiently severe, the force would be sufficient to tear the wings off. The structural analysis must include designating the load factors which may be imposed on the wings under gust loadings at high airspeed.

Recovery and Deployment

The glider, configured as in this design, cannot be deployed from nor recovered into the cargo compartment of the towplane. Future investigation should be done into the use of folding wings. The glider could then be carried in the C-130 and deployed when needed. A wing folding and unfolding mechanism would add flexibility to the design.

Flight Test

A flyable, remote-control model should be built to test the predictions of the performance parameters. Dynamic stability, and performance with towline attached, can be accurately evaluated only by flight test. Stall performance with towline attached and towing characteristics throughout the range of airspeeds and positions are still unknown.

Options for Covert Action

Since the glider is designed to be a covert vehicle, some attention should be given to increasing its effectiveness in covert operations. For example, the glider can be made as a sealed, floating vehicle if desired. In such a case, if the towline were broken for any reason, the vehicle could be flown to any nearby body of water and landed there for later recovery. Calculations have shown that the wing alone half-filled with water could support about 1,400 pounds in salt water.

A balsa wood-foam sandwich could be used in construction rather than metal-foam. Such a structure can be made strong enough to withstand any ordinary in-flight loads. An explosive charge, detonated on command from the towplane, could be used in case of emergency to destroy the payload and burn the airframe.

Improved Aerodynamics

Low airspeed performance falls short of that stated in the orginal specifications. The glider was to have been

flyable down to 15 knots. Redesign for a lighter payload or the use of a different wing section might improve low-speed characteristics.

Professor Larsen has suggested replacing the wheel with a skid. A skid requires no cutting into the fuselage and adds very little drag. He also recommended lengthening the tail section of the fuselage an additional $1\frac{1}{4}$ feet so that it ends parallel to the trailing edge of the horizontal tail. This would allow smoother departure of the airflow at the aft end of the fuselage around the gentler curvature. Both skid and longer fuselage should be investigated in a future cycle of the design.

Bibliography

1. Corning, Gerald. <u>Supersonic and Subsonic Airplane Design</u> (Second Edition). Ann Arbor, Michigan: Edwards Brothers, Inc., 1953.

2. Department of Aeronautics, USAF Academy. "The Finite Wing." Unpublished instructional material in basic aerodynamics. United States Air Force Academy, Colorado: DFAN, 1966.

3. Dittrich, Mark S. <u>Performance, Stability and Control, Volume I and II</u>. United States Air Force Academy, Colorado: Department of Aeronautics, 1969.

4. Dittrich, Mark S. "Static Stability and Control." Unpublished course material in aircraft design. United States Air Force Academy, Colorado: Department of Aeromautics, 1969.

5. Dwinnell, James H. <u>Principles of Aerodynamics</u>. New York: McGraw-Hill Book Company, Inc., 1949.

6. Etkin, Bernard. <u>Dynamics of Flight</u>. New York: John Wiley & Sons, Inc., 1967.

7. Federal Aviation Administration. <u>Flight Training Handbook</u>. AC 61-21. Washington, D.C.: U.S. Government Printing Office, 1965.

8. Flight Control Division, Air Force Dynamics Laboratory. <u>USAF Stability and Control Datcom</u> (Revised Edition). Wright Patterson Air Force Base, Ohio: AFFDL (FDCC), 1969.

9. Jacobs, Eastman N. and Ira H. Abbott. <u>Airfoil Section Data Obtained in the N.A.C.A. Variable-Density Tunnel as Affected by Support Interference and Other Corrections</u>. NACA Report No. 669. Washington, D.C.: U.S. Government Printing Office, 1948.

10. Liepmann, H.W. and A. Roshko. <u>Elements of Gasdynamics</u>. New York: John Wiley & Sons, Inc., 1967.

11. Perkins, Courtland D. and Robert E. Hage. <u>Airplane Performance, Stability and Control</u>. New York: John Wiley & Sons, Inc., 1949.

12. Pope, Alan. <u>Basic Wing Airfoil Theory</u>. New York: McGraw-Hill Book Company, Inc., 1951.

13. Schlichting, Herman. *Boundary Layer Theory* (Fourth Edition). New York: McGraw-Hill Book Company, Inc., 1960.

14. Simons, John C., Lt. Col., USAF, and B. C. Dixon. *Long-Line Loiter: Improvement of Some Free-Fall and Circling-Line Techniques, Volume I.* ASD-TR-69-95. Wright-Patterson Air Force Base, Ohio: Aeronautical Systems Division, 1969.

Appendix A

Shape, Area, and Volume of the Fuselage

The curves which were specified for nose and tail were required to meet the cylindircal main fuselage smoothly, without any abrupt change in curvature. This is a consequence of Crocco's Theorem (Ref 10:191-93) which relates the vorticity in a given flow field to the entropy gradient normal to the streamlines of the flow. Abrupt changes in curvature induce vorticity in the flow. Physically, the vorticity appears as additional drag which in turn results in decreased vehicle performance.

If the second derivative of radius with respect to longitudinal position is forced to vanish where the nose and tail sections meet the cylindrical fuselage, then the smoothness condition is satisfied. The equation for the nose is

$$\left(\frac{x}{a}\right)^n + \left(\frac{y}{b}\right)^n = 1, \qquad n > 2 \qquad (1)$$

The exponent n = 3 was chosen at the designer's option. The length a = 40 in was optional, and the length b = 14 in was dictated by the cylindrical radius. The ordinates were plotted symmetrically up and down from the longitudinal axis using as an origin a station 40 in inward from the nose. For selected stations, x, Table XIII gives the corresponding ordinates.

To find the surface area of a body of revolution, the

Table XIII

Tabulation of Nose Radius for Selected Stations

x, in	y, in	x, in	y, in
0	14.00	30	11.66
2	14.00	31	11.36
4	14.00	32	11.02
6	13.98	33	10.64
8	13.96	34	10.18
10	13.93	35	9.67
12	13.87	36	9.06
14	13.79	37	8.30
16	13.69	38	7.31
18	13.55	39	5.86
20	13.39	39.2	5.34
22	13.17	39.4	4.96
24	12.90	39.5	4.67
26	12.58	39.6	4.33
28	12.17	39.8	3.45
		40	0.00

area of a longitudinal section is multiplied by π (Ref 1:
6:5, 6:6). Simpson's Rule was used for computing the area
between the curve and the longitudinal axis. Doubling this
area gave the area of the entire nose. Table XIV presents
the incremental areas for the lengths given. Adding together
all the incremental areas gave the area of the longitudinal
section of the nose as 989.6 in^2.

The nose volume was computed by dividing the longitudinal
section into increments and finding the volume of each incre-
ment as the volume of a disc. The radius of the disc was
taken as the average of the radii of both faces. Table XV
presents the incremental volumes for each section. Adding
all the discs gave the volume of the nose as 19,850 in^3.

Table XIV

Incremental Areas for Selected Stations

x, in	Area, in^2	x, in	Area, in^2
0-1	28.00	25-27	50.32
1-3	56.00	27-29	48.68
3-5	56.00	29-31	46.64
5-7	55.92	31-31½	11.28
7-9	55.84	31½-32½	22.04
9-11	55.72	32½-33½	21.28
11-13	55.48	33½-34½	20.36
13-15	55.16	34½-35½	19.34
15-17	54.76	35½-36½	18.12
17-19	54.20	36½-37½	16.60
19-21	53.56	37½-38½	14.62
21-23	52.68	38½ 39½	11.72
23-25	51.60	39½-40	3.71

Table XV

Incremental Volumes for Selected Stations

x, in	Vol, in^3	x, in	Vol, in^3
0-1	615	25-27	996
1-3	1230	27-29	930
3-5	1230	29-31	840
5-7	1228	31-31½	200
7-9	1224	31½-32½	382
9-11	1220	32½-33½	356
11-13	1208	33½-34½	326
13-15	1194	34½-35½	294
15-17	1178	35½-36½	258
17-19	1154	36½-37½	217
19-21	1126	37½-38½	168
21-23	1090	38½-39½	108
23-25	1046	39½-40	22

Tail Section

The tail section has been tapered sharply to end in a point on the longitudinal axis. The equation for the tail section was given in Equation (2) and is repeated below:

$$\frac{d^2y}{dx^2} = Kx(1 - x) \tag{2}$$

The length of the tail section was set at 40 in and the radius at 14 in. This fixes the boundary conditions as

$$x = 0 \qquad dy/dx = 0$$
$$x = 40 \qquad y = 14$$

Solving the boundary-value problem gave the expression for y in terms of x as follows:

$$y = \frac{14}{2,432,000} (x^4 - 2 x^3) \tag{4}$$

To plot the tail, the upper and lower surfaces of the fuselage were extended rearward to be used as axes rather than using the longitudinal axis of the fuselage. The origin of coordinates was located on the cylindrical surface at the point where the tail section joined the cylinder. The ordinates were plotted downward toward the longitudinal axis. Table XVI shows ordinates corresponding to selected stations x. The actual height, or distance from the longitudinal axis, was computed by subtracting each value of y from 14.00.

The area of the tail in longitudinal section was found by direct integration. The integral of Equation (4), however, gives the area between the curve and the axis at the cylin-

Table XVI

Tabulation of Tail Radii for Selected Stations

x, in	y, in	Actual Ht, in
0	0.00	14.00
2	0.00	14.00
4	0.00	14.00
6	0.01	13.99
8	0.02	13.99
10	0.05	13.95
12	0.09	13.90
14	0.19	13.81
16	0.33	13.67
18	0.54	13.46
20	0.83	13.17
22	1.23	12.77
24	1.75	12.25
26	2.43	11.57
28	3.29	10.71
30	4.35	9.65
32	5.66	8.34
34	7.24	6.76
36	9.13	4.87
38	11.37	2.63
40	14.00	0.00

drical surface extended rearward. Thus the tail area was found by subtracting the value of the integral from the area of a rectangle 40 in X 14 in and then doubling to obtain both halves. The area of the tail in longitudinal section is 898.9 in^2.

The volume of the tail section was found by Simpson's Rule. Table XVII shows the volumes of incremental discs which use as their radii the average radii of each face of the disc. Summing the increments results in a volume for the tail section of 17,587.4 in^3.

Table XVII

Incremental Volumes for Selected Tail Stations

x, in	Vol, in^3	x, in	Vol, in^3
0-2	1232.0	20-22	1060.0
2-4	1232.0	22-24	982.0
4-6	1232.0	24-26	894.0
6-8	1230.0	26-28	782.0
8-10	1225.0	28-30	668.8
10-12	1222.0	30-32	507.0
12-14	1208.0	32-34	360.6
14-16	1182.0	34-36	212.4
16-18	1154.0	36-38	88.6
18-20	1114.0	38-40	10.8

Cylindrical Main Fuselage

The cylinder has a length of 106 in and a constant radius of 14 in. The area of the longitudinal section is 2968 in^2. The volume of the cylinder is 65,237 in^3.

Vehicle Volume and Surface Areas

Adding the contributions of the nose, tail, and cylindrical main fuselage gives the areas and volume of the entire fuselage. They are as follows:

Longitudinal section area	4856.6 in^2
Fuselage gross surface area	15,249.7 in^2
Fuselage volume	102,674 in^3

Appendix B

Lift Distribution by Schrenk's Method

An accurate and convenient method for determining the lift distribution along the span of a nonelliptic wing was presented by Otto Schrenk in 1940. When the wing is non-elliptic, the downwash varies along the span. Schrenk's Method allows conpensation for this varying downwash. It assumes that the final span load distribution for an untwisted wing is halfway between the geometric planform shape and the shape of a semi-ellipse of the same area. The solution can then be modified to account for the effects of twist. The assumption is very reasonable in practice, but it does not follow directly from theory (Ref 12:255).

The spanwise lift distribution may be divided into two parts:

1. The additional lift distribution which is that part of the lift due to angle of attack. It is referred to the wing zero-lift angle.

2. The basic lift distribution which occurs when the wing lift coefficient is zero. This component exists only when the wing is twisted aerodynamically.

The total lift distribution of the wing is the sum of the two contributions (Ref 12:255).

The following assumptions must be satisfied for the Schrenk Method to yield accurate results:

1. The additional lift distribution for a wing lift coefficient of 1.0 is halfway between the actual distribution of the wing chord and the chord of a semi-ellipse having the same area as the wing.

2. The basic lift distribution is found halfway between the lift distribution referred to the wing zero-lift line and the geometric lift coefficient due to twist.

3. As the center of lift is moved outward, the non-dimensional spanwise lift distribution coefficient is reduced by some function of the angle of sweepback (Ref 12:256).

The additional lift distribution (at $C_L = 1.0$) is denoted by $cc_{l_{al}}$, and it may be found as follows: The wing area is set equal to half the area of an ellipse whose semi-minor axis is equal to $4S_W/\pi b$ and whose semi-major axis is equal to $b/2$. The equation for the ellipse is then

$$\frac{x^2}{(4S_W/\pi b)^2} + \frac{y^2}{(b/2)^2} = 1.0 \qquad (55)$$

Y is plotted outward along the span. The length of the elliptic chord, c_e, is given by the values of x. Assuming that the value of $cc_{l_{al}}$ is the mean between the actual wing chord, c, and the elliptical wing chord, the additional lift distribution for any span station is given by

$$cc_{l_{al}} = \frac{c}{2} + \frac{2 S_W}{\pi b} \sqrt{1 - \left(\frac{2y}{b}\right)^2} \qquad (56)$$

This lift distribution is for a wing lift coefficient of unity. The actual additional lift distribution for the wing

at any other wing lift coefficient, C_L, is given by

$$cc_{l_a} = C_L \left[\frac{c}{2} + \frac{2\,S_W}{\pi\,b} \sqrt{1 - \left(\frac{2y}{b}\right)^2} \right] \quad (57)$$

Correction for variable thickness ratio may be made as follows: Let a_0 be the local slope of the lift curve and $\bar{a}_0$ be the average slope of the lift curve for the half-span. Equation (57) is corrected to read

$$cc_{l_{ax}} = C_L \left[\frac{c}{2} \frac{a_0}{\bar{a}_0} + \frac{2\,S_W}{\pi\,b} \sqrt{1 - \left(\frac{2y}{b}\right)^2} \right] \quad (58)$$

and the definition of $\bar{a}_0$ is

$$\bar{a}_0 = \frac{2}{S} \int_0^{b/2} c\, a_0 \, dy \quad (59)$$

To the additional lift distribution must be added the basic lift distribution. Let ϵ_0 designate the section twist angle referred to the wing zero-lift line. The angle of zero lift is given by

$$\alpha_{ZL} = \frac{2}{S} \int_0^{b/2} \epsilon_0 \, c \, dy \quad (60)$$

For equal total lifts, a twisted wing must have a higher value of circulation at the centerline than has an untwisted wing. Trailing edge vortices shed by the twisted wing before the tip region have a greater total value than they do for the untwisted wing. The shed vortices have the effect of increasing the angle of attack at the wingtip. This effect essentially acts to reduce the twist that made the vortices. A 50% reduction in effect of twist is a good approximation. Therefore, the basic lift distribution is given by

$$c_{1_b} = \frac{\epsilon_o - \alpha_{ZL}}{2} \, a_o \qquad (61)$$

The net lift distribution across the twisted wing for a C_L other than unity was given by Equation (6), repeated below, modified to accommodate a variable wing chord.

$$cc_1 = C_L \left[\frac{c}{2} \frac{a_o}{\bar{a}_o} + \frac{2 \, S_W}{\pi b} \sqrt{1 - \left(\frac{2y}{b}\right)^2} \right] + \frac{\left(\epsilon_o - \alpha_{ZL}\right)}{2} a_o c$$

$$(62)$$

For the wing used in this design, the basic lift distribution is zero. When Equation (62) is divided by the value of the constant chord, c, Equation (6) results. Equation (6) was used to generate the values for section lift coefficient plotted in Figure 5.

The development of the Schrenk Method in this Appendix follows the presentation of Pope (Ref 12:255-58).

Appendix C

Computation of the Wetted Areas

The combined vehicle drag characteristics were found by
the wetted area method. The wetted area is that part of the
gross surface area which is exposed to the airstream. This
Appendix discusses the simplifications which were made in
order to find areas made up of intersections of curved
surfaces.

Wetted Area of the Fuselage

The lengths of the curved surfaces of the wing inter-
section were approximated by straight lines. These lines
were drawn from the leading and trailing edges to meet on the
centerline at the top of the vehicle one-third chord behind
the leading edge. Two triangles were thus formed which lay
diagonally through the thickness of the wing. The maximum
thickness cut out of the fuselage is equal to the wing
thickness, 4.32 in. The slant height of each triangle was
found to be 11.0 in. The total area of the two traingles
was found to be 396 in^2.

Area was also removed from the fuselage due to the ver-
tical tail, horizontal tail, tow hitch, wheel, and antenna.
To compute the amount removed by the vertical tail, the curved
tail section intersection was approximated by a straight
line drawn between the intersection points of the fuselage
with the leading edge and hingeline of the vertical tail.

The base area of the tail was plotted to scale and projected onto the oblique line. The wetted area reduction due to the fin was thus found to be 69.1 in^2.

To find the area reduction due to the horizontal tail, it was assumed that one-half of the 2.5 ft chord was in contact with the fuselage. The combined area reduction due to intersection with the horizontal tail is 54.7 in^2.

The amount of area reduction due to the wheel, tow hitch, and antenna was estimated to be 25 in^2, 4 in^2, and 4 in^2, respectively.

Subtracting each of these individual area reductions gave the fuselage wetted area as 14,727.6 in^2.

Wetted Area of the Wing

Only the area due to intersection with the fuselage is removed from the gross surface area of the wing. A rectangular panel on the bottom measuring 20.4 in X 36.3 in removes 740 in^2. The curved top of the wing was represented by two triangular panels which lay next to the two panels discussed previously. The total area of the two triangular and one rectangular panels was found to be 1655.6 in^2. The remaining wetted area of the wing was then found to be 25,298.2 in^2.

Wetted Area of the Horizontal Tail

The amount of area removed from the horizontal tail was due solely to intersection with the fuselage. The inboard airfoils were laid out to scale and the areas com-

puted by Simpson's Rule. The amount of area removed by intersection was taken to be one-half the area of the inboard tips on each side, an area which totaled 54.7 in^2. Subtracting from the gross area gave the wetted area as 4828.1 in^2.

Wetted Area of the Vertical Tail

Figure 7 shows that portions of both sides and the bottom of the vertical tail are intersected by the fuselage. The lateral area was assumed to be triangular, the curve of the fuselage being approximated by a straight line. The amount of lateral area removed was estimated from a scale drawing. For both sides it is 253.6 in^2. The area of the bottom was computed from a scale drawing of the base airfoil and found to be 76.6 in^2. Subtracting these areas from the gross area of the vertical tail gave the wetted area as 2317.8 in^2.

Wetted Area of the Wheel

The wheel was presumed to be 8 in in diameter, 2 in thick, and half exposed. The wetted area follows directly: 75.5 in^2.

Wetted Areas of Tow Hitch and Antenna

The areas of the tow hitch and antenna are not known. They were assumed to be 4 in^2 and 20 in^2, respectively.

Vita

Elbridge Lee Snapp, III, was born 3 December 1944 in Philadelphia, Pennsylvania. He graduated from the Forrest Sherman High School in Naples, Italy, in June 1962. In September 1962 he entered the University of Maryland, College Park, Maryland. Appointed to the United States Air Force Academy in 1965, he graduated in 1969 with a Bachelor of Science in Aeronautical Engineering. During his tenure at the Academy he earned his FAA Flight Instructor (Glider), Commercial Pilot (Glider), and Ground Instructor (Advanced and Instrument) Certificates. He has written A Handbook on Soaring for the Commercial Pilot and co-authored the Basic Soaring Textbook, both published at the Air Force Academy. In 1969 he entered the Air Force Institute of Technology to pursue studies toward a Master of Science in Astronautics.

Home Address: 600 Perth Place
                      Silver Spring, Maryland 20901